Local axonal function of STAT3 rescues axon degeneration in the *pmn* model of motoneuron disease

Bhuvaneish Thangaraj Selvaraj,[1] Nicolas Frank,[1] Florian L.P. Bender,[1] Esther Asan,[2] and Michael Sendtner[1]

[1]Institute for Clinical Neurobiology and [2]Institute of Anatomy and Cell Biology, University of Wuerzburg, 97078 Wuerzburg, Germany

Axonal maintenance, plasticity, and regeneration are influenced by signals from neighboring cells, in particular Schwann cells of the peripheral nervous system. Schwann cells produce neurotrophic factors, but the mechanisms by which ciliary neurotrophic factor (CNTF) and other neurotrophic molecules modify the axonal cytoskeleton are not well understood. In this paper, we show that activated signal transducer and activator of transcription-3 (STAT3), an intracellular mediator of the effects of CNTF and other neurotrophic cytokines, acts locally in axons of motoneurons to modify the tubulin cytoskeleton. Specifically, we show that activated STAT3 interacted with stathmin and inhibited its microtubule-destabilizing activity. Thus, ectopic CNTF-mediated activation of STAT3 restored axon elongation and maintenance in motoneurons from *progressive motor neuronopathy* mutant mice, a mouse model of motoneuron disease. This mechanism could also be relevant for other neurodegenerative diseases and provide a target for new therapies for axonal degeneration.

Introduction

In most neurodegenerative diseases, periods of clinically silent alterations precede the first symptoms. Synaptic dysfunction and loss are thought to occur early but are compensated by sprouting of neighboring axon terminals (Cafferty et al., 2008; Giger et al., 2010). For example, in $Smn^{+/-}$ mice, a model of mild forms of spinal muscular atrophy, >50% of the motoneuron cell bodies are lost, and intensive ciliary neurotrophic factor (CNTF)–dependent sprouting occurs before disease becomes clinically apparent (Simon et al., 2010). Axonal degeneration often starts with alterations in distal axons and presynaptic terminals (Pun et al., 2006), leading to morphological degeneration that normally sets the stage for irreversible alterations that finally lead to neuronal cell death. Axonal degeneration marks the transition from early disease stages when regeneration in principle is possible (Cafferty et al., 2008) and late stages when the pathological alterations are so severe that challenges for effective treatment become insurmountable.

In animal models of motoneuron disease, neuromuscular endplates are lost early (Pun et al., 2006), and pathological alterations in axons normally precede the cell death of spinal motoneurons (Sendtner et al., 1992). Because axons of motoneurons are easily accessible, motoneuron disease models appear as an ideal tool for studying molecular mechanisms of axonal degeneration and disease progression in neurodegeneration. These mechanisms appear important not only for motoneuron disease but for a much broader spectrum of neurodegenerative disorders in which axons degenerate and could guide the development of therapies for such diseases.

A large body of evidence, mainly coming from human genetic experiments and from the analysis of mouse models, points to axonal trafficking and vesicle sorting/transport as critical targets of disease mechanisms in motoneuron diseases (Hafezparast et al., 2003). First, mutations in genes for components of kinesin complexes that are necessary for anterograde axonal transport, i.e., KIF1B-β and KIF5A, are associated with various forms of motoneuron disease, such as hereditary spastic paraplegy (SPG10) and Charcot-Marie-Tooth type 2A

B.T. Selvaraj and N. Frank contributed equally to this paper.

Correspondence to Michael Sendtner: sendtner@mail.uni-wuerzburg.de

Abbreviations used in this paper: ANOVA, analysis of variance; BDNF, brain-derived neurotrophic factor; bFGF, basic FGF; CNTF, ciliary neurotrophic factor; DIV, day in vitro; GAPDH, glyceraldehyde 3-phosphate dehydrogenase; GDNF, glial-derived neurotrophic factor; KO, knockout; LIF, leukemia inhibitory factor; MT, microtubule; MTOC, MT-organizing center; NFL, neurofilament; *pmn*, *progressive motor neuronopathy*; shRNA, short hairpin RNA; STAT3, signal transducer and activator of transcription-3.

The Rockefeller University Press $30.00
J. Cell Biol. Vol. 199 No. 3 437–451
www.jcb.org/cgi/doi/10.1083/jcb.201203109

(Zhao et al., 2001; Reid et al., 2002). Second, mice in which dynamitin is overexpressed (LaMonte et al., 2002), and which, as a result, have disturbed retrograde axonal transport, or mice with mutation in dynein heavy chain 1 (LOA [legs at odd angles] and Cra1 [cramping1] mice; Hafezparast et al., 2003) develop symptoms that are similar to motoneuron disease (LaMonte et al., 2002; Andersen, 2003; Hafezparast et al., 2003; Puls et al., 2003). A mutation in the p150 subunit of dynactin has also been found in a family with a slowly progressive autosomal dominant form of motoneuron disease with vocal cord paralysis (Puls et al., 2003). Third, the underlying gene defect in the *wobbler* mouse, a classical mouse model of motoneuron disease, inactivates the VPS54 protein, which is important for cellular vesicle sorting (Schmitt-John et al., 2005). Fourth, modulation of neurofilaments (NFLs) and the resulting disturbed stoichiometry of filamentous structures in the axon lead to motoneuron disease in transgenic mouse models (Collard et al., 1995). Moreover, the underlying gene defect in the *progressive motor neuronopathy* (*pmn*) mouse, another mouse model of amyotrophic lateral sclerosis, affects the activity of tubulin-specific chaperone E and, by this means, the assembly of microtubules (MTs; Bommel et al., 2002; Martin et al., 2002), which seems to play a key role for axonal trafficking and axonal stability.

pmn mutant mice suffer from a severe form of motoneuron disease. First symptoms of weakness appear in the third postnatal week. The mice then die within the following 3 wk. The disease is caused by a point mutation (t1682g) in the *Tbce (tubulin-specific chaperone E*, *cofactor E*) gene. This mutation leads to an amino acid exchange of tryptophan to glycine (W524G) at the most C-terminal position of the protein. The mutation destabilizes the TBCE protein (Bommel et al., 2002; Martin et al., 2002), but it does not completely abolish its enzymatic activity because MTs are present in most types of cells, and mitosis that depends on intact MTs for the spindle apparatus is not affected in the developing *pmn* mutant mice. The same mutation or mutations in the last coding exon of *Tbce* have not been found in >700 patients with sporadic and familial forms of motoneuron disease (unpublished data). Mutations in other regions of the *Tbce* gene that abolish the enzymatic activity of the corresponding protein (c.155-166del12; p.del 52–55) have been associated with the hypoparathyroidism–retardation–dysmorphism syndrome (Parvari et al., 2002), a rare autosomal recessive disorder characterized by short stature as a result of growth hormone insufficiency, mental retardation, facial dysplasia, and endocrinological defects, such as hypocortisolemia. In contrast, the W524G mutation found in *pmn* mutant mice gives rise to a disease in which destabilized Tbce protein results in unstable MTs that causes a neurodegenerative disease that predominantly affects motoneurons (Bommel et al., 2002; Martin et al., 2002).

Cell death of motoneuron cell bodies appears as a consequence of axonal degeneration (Sendtner et al., 1992; Bommel et al., 2002). When bcl-2 is overexpressed in motoneurons of *pmn* mutant mice, cell death of motoneuron cell bodies is prevented, but this has no influence on disease onset or progression because axon degeneration is not positively affected by the bcl-2 transgene (Sagot et al., 1995). Similarly, treatment with the neurotrophic factor glial-derived neurotrophic factor (GDNF) only prevents loss of motoneuron cell bodies but does not influence axonal degeneration (Sagot et al., 1996) or retrograde axonal transport (Sagot et al., 1998), a functional consequence of the axonal degeneration. In contrast, treatment with the neurotrophic factor CNTF significantly delays disease onset and prolongs survival of *pmn* mice (Sendtner et al., 1992, 1997). This difference appears surprising because CNTF and GDNF are potent survival factors for motoneurons, both in vitro and in vivo. This observation therefore raises the question on the molecular basis how CNTF, but not GDNF, rescues axons.

Here, we show that CNTF, in contrast to GDNF or brain-derived neurotrophic factor (BDNF), rescues axonal degeneration via a pathway involving signal transducer and activator of transcription-3 (STAT3) and stathmin. Most of the activated STAT3 protein is not transported to the nucleus to activate transcription but interacts locally in axons with stathmin, a protein that destabilizes MTs. This interaction plays a major role in CNTF signaling for MT dynamics in axons. Thus, the STAT3–stathmin pathway could be a potent target for therapy development in motoneuron disease.

Results

CNTF, but not BDNF or GDNF, rescues axonal pathology in *pmn* mutant motoneurons

CNTF influences synaptic and axonal degeneration in a variety of mouse models (Sendtner et al., 1992; Mitsumoto et al., 1994; Pun et al., 2006). In superoxide dismutase G93A mice, it prevents pruning and loss of synaptic vesicles at neuromuscular endplates (Pun et al., 2006), and in *pmn* mutant mice, the severe paralysis and respiratory failure can be significantly delayed by systemic CNTF treatment (Sendtner et al., 1992). Interestingly, GDNF, another potent survival factor for motoneurons (Henderson et al., 1994), cannot prevent synaptic pruning and axon degeneration in the superoxide dismutase G93A and the *pmn* mouse models (Sagot et al., 1996). To investigate the underlying mechanism for this difference, we compared the effects of BDNF, GDNF, and CNTF in cultured embryonic motoneurons from control and *pmn* mutant mice. Although these three neurotrophic factors were equally potent in supporting motoneuron survival (Fig. S1), both in wild-type and *pmn* mutant motoneurons, they differed significantly with respect to their effects on axon growth (Fig. 1, A and B). After 7 d in culture, each of these factors promoted axon elongation in wild-type motoneurons to ∼1,000–1,300 µm. However, axons of *pmn* mutant motoneurons were significantly shorter with BDNF or GDNF but not with CNTF (Fig. 1 B). Furthermore, CNTF, but not BDNF or GDNF, reduced the number of axonal swellings that are characteristic for *pmn* mutant motoneurons (Fig. 1 C; Bommel et al., 2002). Ultrastructural analysis also revealed reduced MT density in axons of *pmn* mutant mice (Fig. 1 D), confirming a previous study (Schaefer et al., 2007). However, the reduction of MT density was less than expected in distal regions and reached statistical significance only in the proximal axons (Fig. S2). The axonal swellings in axons in *pmn*

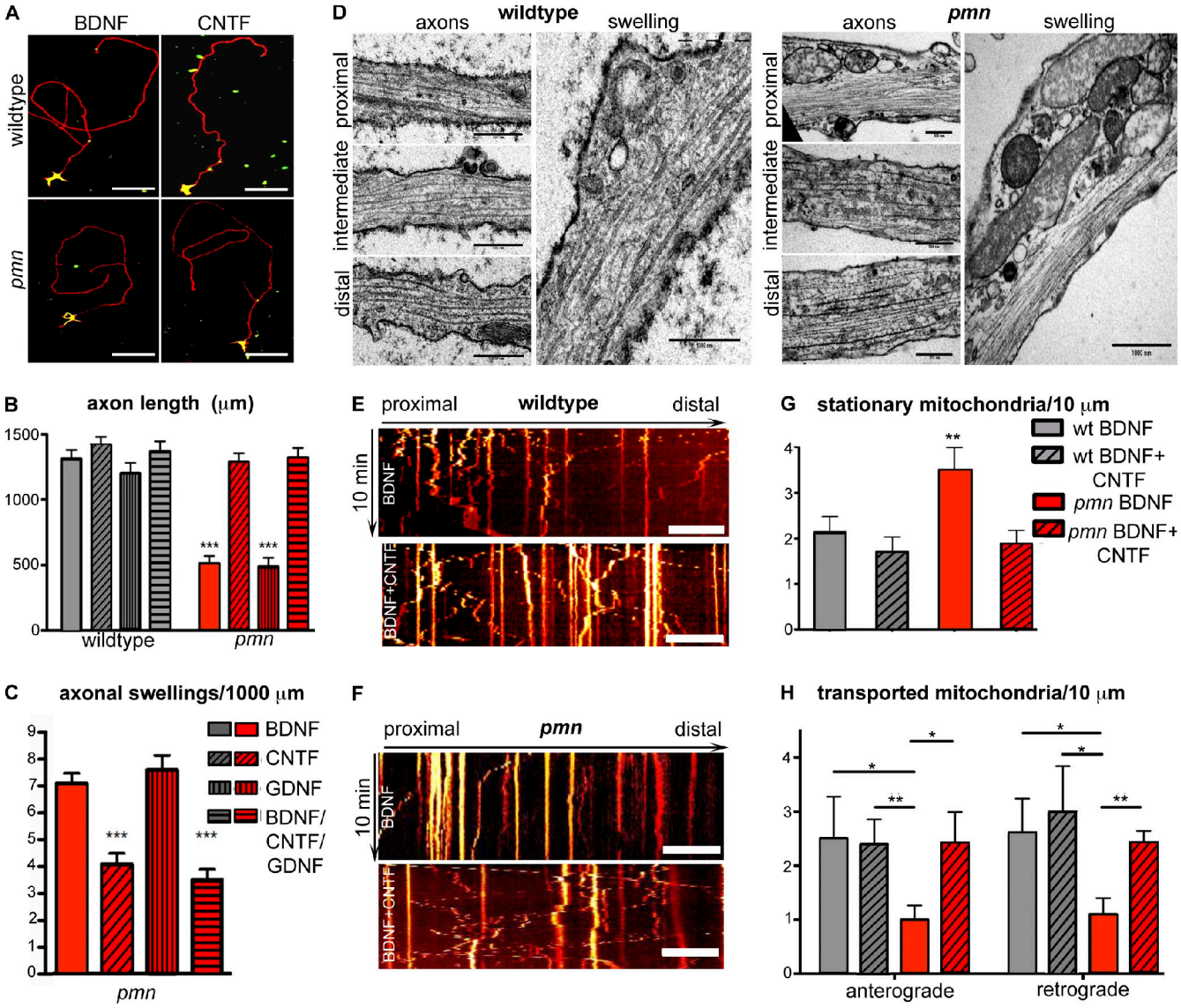

Figure 1. **CNTF rescues axon elongation and mitochondrial transport in *pmn* mutant motoneurons in vitro.** (A) Representative images of *pmn* mutant and wild-type motoneurons cultured for 7 DIV in the presence of BDNF or CNTF and stained against MAP2 (green) and against tau (red). Bars, 100 µm. (B and C) Differential effect of CNTF on axon length and reduction in axonal swellings. $n = 3$ independent experiments. At least 50 cells were measured per condition and experiment. (D) Electron micrographs of axonal segments (left) and swellings (right) of wild-type and *pmn* mutant motoneurons cultured in presence of BDNF for 7 DIV, showing swellings filled with organelles in *pmn* mutant motoneurons. Bars: (left) 500 nm; (right) 1,000 nm. (E and F) Representative kymographs of axonal mitochondria labeled with Rhodamine 123 in wild-type and *pmn* mutant motoneurons cultured for 5 DIV in the presence of BDNF or BDNF and CNTF. Bars, 25 µm. (G and H) CNTF normalizes axonal transport of mitochondria in *pmn* mutant (54 cells for 5 ng/ml BDNF and 19 cells for 10 ng/ml BDNF + CNTF) motoneurons to levels in wild-type motoneurons (28 cells for BDNF and 12 cells for BDNF + CNTF). $n = 6$ independent experiments. Statistical analysis: *, $P < 0.05$; **, $P < 0.01$; ***, $P < 0.001$; ANOVA with Bonferroni posthoc test. wt, wild type. Data shown represent means ± SEM.

mutant motoneurons include high numbers of mitochondria (Fig. 1 D, right). Therefore, we labeled motoneurons with the fluorescent dye Rhodamine 123 and found that CNTF, but not BDNF, decreased the number of stationary mitochondria in *pmn* mutant motoneurons (Fig. 1, E–G). Conversely, the number of mitochondria that were transported into the anterograde or retrograde direction increased to wild-type levels in the presence of CNTF and BDNF (Fig. 1 H) but not BDNF alone. The maximum speed of axonal transport of mitochondria in the anterograde direction was lower in *pmn* mutant motoneurons in comparison to wild type and increased to wild-type levels by CNTF (Fig. S3 A). The number of mitochondria in axons of wild-type and *pmn* mutant motoneurons was not different (Fig. S3 B). These effects of CNTF on enhancing rate and speed of axonal transport were specific for *pmn* mutant motoneurons. No differences in mitochondrial transport were observed with BDNF and CNTF in wild-type motoneurons.

STAT3 is necessary for CNTF effects on axons in *pmn* mutant motoneurons

BDNF and GDNF mediate their effects on motoneuron survival and axon growth through the transmembrane tyrosine kinase receptors TrkB and c-ret, respectively. In contrast, CNTF modulates these functions through a cytokine receptor involving the

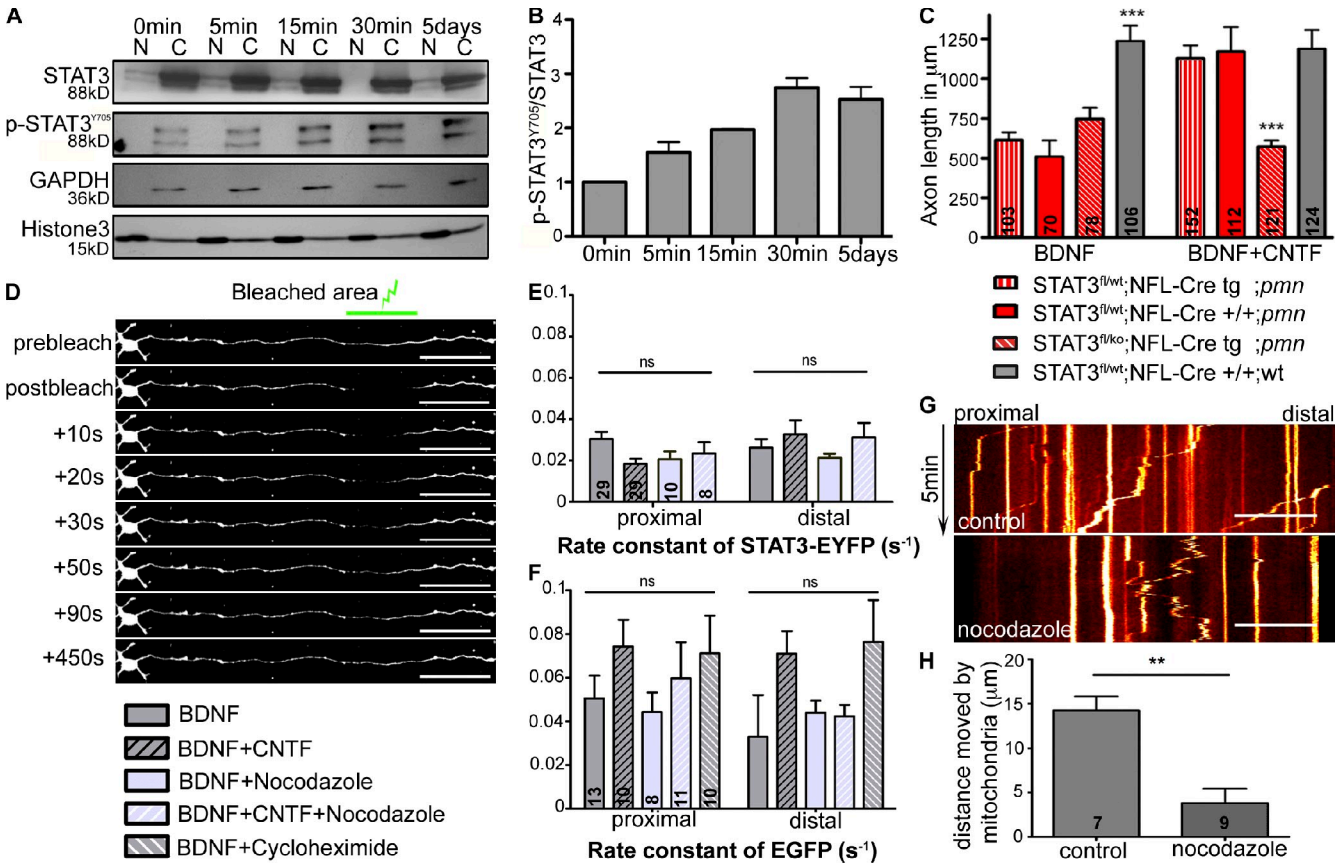

Figure 2. **STAT3 is essential for CNTF-mediated axon elongation.** (A) Nuclear (N) and cytoplasmic (C) fractionation followed by Western blot analysis from primary motoneurons showing activation of p-STAT3^{Y705} upon CNTF stimulation. Activated STAT3 is mainly found in the cytoplasm at any time point investigated. Fractionation was controlled with GAPDH (cytosolic) and histone 3 (nuclear) as markers. (B) Quantification of activated p-STAT3^{Y705} in the cytoplasmic fraction of motoneurons after CNTF stimulation. *n* = 3 independent experiments. For each individual experiment, the 0-min data point was set to 1. (C) Loss of CNTF-mediated rescue of axon length in conditional STAT3 ablated *pmn* mutant motoneurons. Numbers in bars indicate number of cells measured. *n* = 3 independent experiments. Statistical analysis: ***, P < 0.001; ANOVA with Bonferroni posthoc test. (D) Representative images of a FRAP experiment performed on STAT3-EYFP–transduced primary motoneurons cultured for 6 DIV. The bleached axonal segment is marked by the green bar in the first top image. Fluorescence recovery is depicted at various time intervals as shown. For better representation of the montage, motoneuron topology was altered using ImageJ tool straighten. Bars, 100 µm. (E and F) Diffusion rates (s^{-1}) of STAT3-EYFP and EGFP in lentivirally transduced primary motoneurons. Diffusion rates were obtained by curve fitting using one-phase decay function and least-square fit of normalized FRAP data (see Materials and methods). Numbers in bars indicate numbers of cells analyzed. *n* = 3 independent experiments. P > 0.05; Kruskal-Wallis with Dunn's multiple comparison test. (G and H) Acute treatment with 10 µM nocodazole inhibits axonal transport of MitoTracker CMXRos–labeled mitochondria. (G) Representative kymograph of nocodazole-treated motoneurons showing reduced mobility of mitochondria. (H) Quantification of the maximal distance of mitochondrial movement within 5 min. *n* = 3 independent experiments. Numbers in bars indicate numbers of cells analyzed. Statistical analysis: **, P < 0.01; Student's *t* test. Bars, 10 µm. Data shown represent means ± SEM.

glycosylphosphatidylinositol-linked CNTFR-α and LIFR-β and gp130 as transmembrane receptor subunits (Davis and Yancopoulos, 1993). Binding of CNTF to this receptor complex results in activation of cytosolic tyrosine kinases of the Janus kinase family and activation of STAT3 through phosphorylation at tyrosine 705 (Y705). CNTF addition as a pulse to cultured motoneurons results in rapid phosphorylation of STAT3 at Y705, and also continuous exposure to CNTF for 5 d in vitro (DIV) results in STAT3 activation (Fig. 2, A and B). Therefore, we investigated whether STAT3 is responsible for CNTF-mediated effects on *pmn* mutant motoneurons. We generated STAT3$^{KO/wt}$;NFL-Cre$^{tg/tg}$;*pmn*$^{+/-}$ and STAT3$^{fl/fl}$;*pmn*$^{+/-}$ mice and crossbred them to delete STAT3 in *pmn* mutant motoneurons, using the same breeding scheme as described previously (Schweizer et al., 2002). CNTF-mediated rescue of axonal elongation was abolished when STAT3 was depleted from *pmn*$^{-/-}$ motoneurons (Fig. 2 C). In the presence of CNTF, axon length of STAT3$^{fl/KO}$;NFL-Cre^{tg};*pmn*$^{-/-}$ motoneurons was reduced by >50% when compared with wild-type and *pmn* mutant motoneurons that were cultured with CNTF. One functional copy of STAT3 was sufficient to rescue axon length (STAT3$^{fl/wt}$;NFL-Cre^{tg};*pmn*$^{-/-}$) in the presence of CNTF.

We then investigated how much of the activated STAT3 moves to the nucleus when CNTF was added as a pulse for 5, 15, and 30 min, or continuously for 5 d, by fractionating motoneuron cell extracts. Surprisingly, STAT3 phosphorylated at Y705 remained almost quantitatively in the cytoplasm, and very little STAT3 could be detected in the nucleus at any time after CNTF treatment (Fig. 2, A and B) in motoneurons, indicating that the effects of CNTF-activated STAT3 on axons of *pmn* mutant motoneurons could involve a local effect in the axonal cytoplasm rather than a mechanism involving nuclear transcription.

To obtain additional evidence that STAT3 acts locally after activation in axons, we developed lentiviral vectors for transduction of EYFP-labeled STAT3 into cultured motoneurons. Motoneurons were transduced with the STAT3-EYFP construct, an area of 100 µm length within the axon was bleached, and the rate of anterograde and retrograde movement of labeled STAT3 into the bleached area was measured after CNTF addition (Fig. 2, D and E). Lentivirus expressing EGFP that was not coupled to any other protein served as a control (Fig. 2 F). FRAP was used to determine the mobility and direction of movement of EGFP and STAT3-EYFP fusion protein into 20-µm segments proximal and distal within the bleached axon region. There was no significant increase of movement of STAT3-EYFP from the distal part of the axon into the bleached area, indicating that activation of STAT3 did not result in quantitative retrograde movement of this signaling molecule toward the cell body and the nucleus. Mobility of EGFP used as a control (Fig. 2 F) was generally higher than that of the STAT3-EYFP fusion protein, most likely because of the higher molecular mass of the fusion protein. Interestingly, CNTF enhanced mobility of EGFP in the axon (Fig. 2 F), both in the proximal and distal segment. Treatment with nocodazole reduced enhanced mobility, both of EGFP and also of mitochondria (Fig. 2, G and H), indicating that the effect of CNTF depends on intact MTs.

STAT3-dependent rescue of axon growth in *pmn* mutant motoneurons is transcription independent

Because most of the activated STAT3 is not retrogradely transported after CNTF treatment, we analyzed whether CNTF-mediated transcriptional activity is required to rescue axon growth in *pmn* mutant motoneurons. Therefore, we blocked transcription in *pmn* mutant motoneurons using actinomycin D at a concentration of 5 nM to test whether CNTF could still rescue axonal elongation under such conditions. Cultured wild-type and *pmn* mutant motoneurons were treated with actinomycin D at 4 DIV, and axon elongation at 5 DIV was measured (Fig. 3 A). Treatment with actinomycin D <10 nM between day 3 and 5 in culture did not affect the survival of motoneurons (Fig. S4). Wild-type motoneurons showed reduced axon elongation with actinomycin D. In *pmn* mutant motoneurons, the CNTF-mediated rescue of axon elongation was not abolished by actinomycin D, providing further evidence that CNTF signaling for effects on axon pathology in *pmn* mutant motoneurons does not rely on the transcriptional effects of STAT3.

We then generated a lentiviral construct for mutant $STAT3^{EE434–435AA}$-EYFP by site-directed mutagenesis. This mutation abolishes the DNA binding activity but can be activated and phosphorylated at Y705 (Horvath et al., 1995). $STAT3^{Y705F}$-EYFP, which cannot be phosphorylated by CNTF stimulation, was used as a control. Lentiviral transduction of these mutants in primary motoneurons showed that $STAT3^{Y705F}$-EYFP completely abolishes phosphorylation at Y705. Both $STAT3^{wt}$-EYFP and $STAT3^{EE434–435AA}$-EYFP can be activated by CNTF and phosphorylated at Y705 (Fig. 3 B). To test whether $STAT3^{EE434–435AA}$-EYFP abolishes STAT3-dependent transcription, we exploited leukemia inhibitory factor (LIF)–mediated GFAP expression in embryonic day 12 (E12) mouse forebrain neural stem cells. Transcriptional activity of STAT3 is necessary for generating GFAP-positive astrocyte-like cells from these cultures (Rajan and McKay, 1998). As expected, $STAT3^{EE434–435AA}$-EYFP repressed GFAP expression in cultured neural stem cells (Fig. 3 C). As a control, galiellalactone, a transcriptional inhibitor of STAT3, was used at 10 µM, and this treatment also blocked GFAP induction in these cells. To investigate whether STAT3 transcriptional activity is required for axon extension, we analyzed STAT3-deficient *pmn* mutant motoneurons ($STAT3^{fl/KO}$;NFL-Cre^{tg};$pmn^{-/-}$) transduced with $STAT3^{EE434–435AA}$-EYFP, $STAT3^{Y705F}$-EYFP, and $STAT3^{wt}$-EYFP lentiviruses. STAT3-deficient *pmn* mutant motoneurons ($STAT3^{fl/KO}$;NFL-Cre^{tg};$pmn^{-/-}$) cultured with BDNF alone showed shorter axons when compared with wild-type littermates. Overexpression of $STAT3^{wt}$-EYFP (control) and $STAT3^{EE434–435AA}$-EYFP completely rescued CNTF-dependent axon growth in $STAT3^{fl/KO}$;NFL-Cre^{tg};$pmn^{-/-}$ motoneurons, showing that transcriptional activity is not required for this effect. Overexpression of $STAT3^{Y705F}$-EYFP was not capable of rescuing axon outgrowth, thus providing further evidence that STAT3 activation is necessary, but not its transcriptional activity, for CNTF-mediated rescue of axon growth in *pmn* mutant motoneurons (Fig. 3, D and E).

STAT3–stathmin interaction mediates axonal CNTF effects in *pmn* mutant motoneurons

Stathmin is a MT-destabilizing protein that binds to free α/β-tubulin heterodimers and thereby reduces the pool of available tubulin subunits for MT elongation (Amayed et al., 2002). STAT3 has previously been shown in nonneuronal cells to interact with the C terminus of stathmin (Verma et al., 2009), thereby antagonizing its MT-destabilizing activity (Ng et al., 2006). This interaction is enhanced upon STAT3 phosphorylation at Y705 (Verma et al., 2009). Therefore, we investigated whether stathmin is involved in CNTF-STAT3–mediated rescue of axonal pathology in cultured *pmn* mutant motoneurons. We first investigated the localization of stathmin and STAT3 in cultured motoneurons and found that these two proteins are colocalized in axons (Fig. 4 A), in cell bodies, and dendrites (Fig. S5 A). To test whether CNTF-dependent activation of STAT3 results in enhanced binding to stathmin, we cultured motoneurons for 4 DIV in the presence of 5 ng/ml BDNF, deprived the cultures overnight of serum, and stimulated them the next day with 10 ng/ml CNTF for 30 min. We then immunoprecipitated stathmin and tested the levels of coprecipitated STAT3. STAT3 interaction with stathmin increased more than twofold in CNTF-treated cultures when compared with controls treated with BDNF only (Fig. 4, B and C). We also tested whether stathmin interaction with tyrosinated α-tubulin is altered by CNTF application. This interaction was reduced after CNTF treatment (Fig. 4, B and C), indicating that CNTF-dependent interaction of STAT3 with stathmin leads to a release of stathmin-bound α/β-tubulin heterodimers.

We then determined whether STAT3 phosphorylation at Y705 is required for interaction with stathmin. Stathmin was

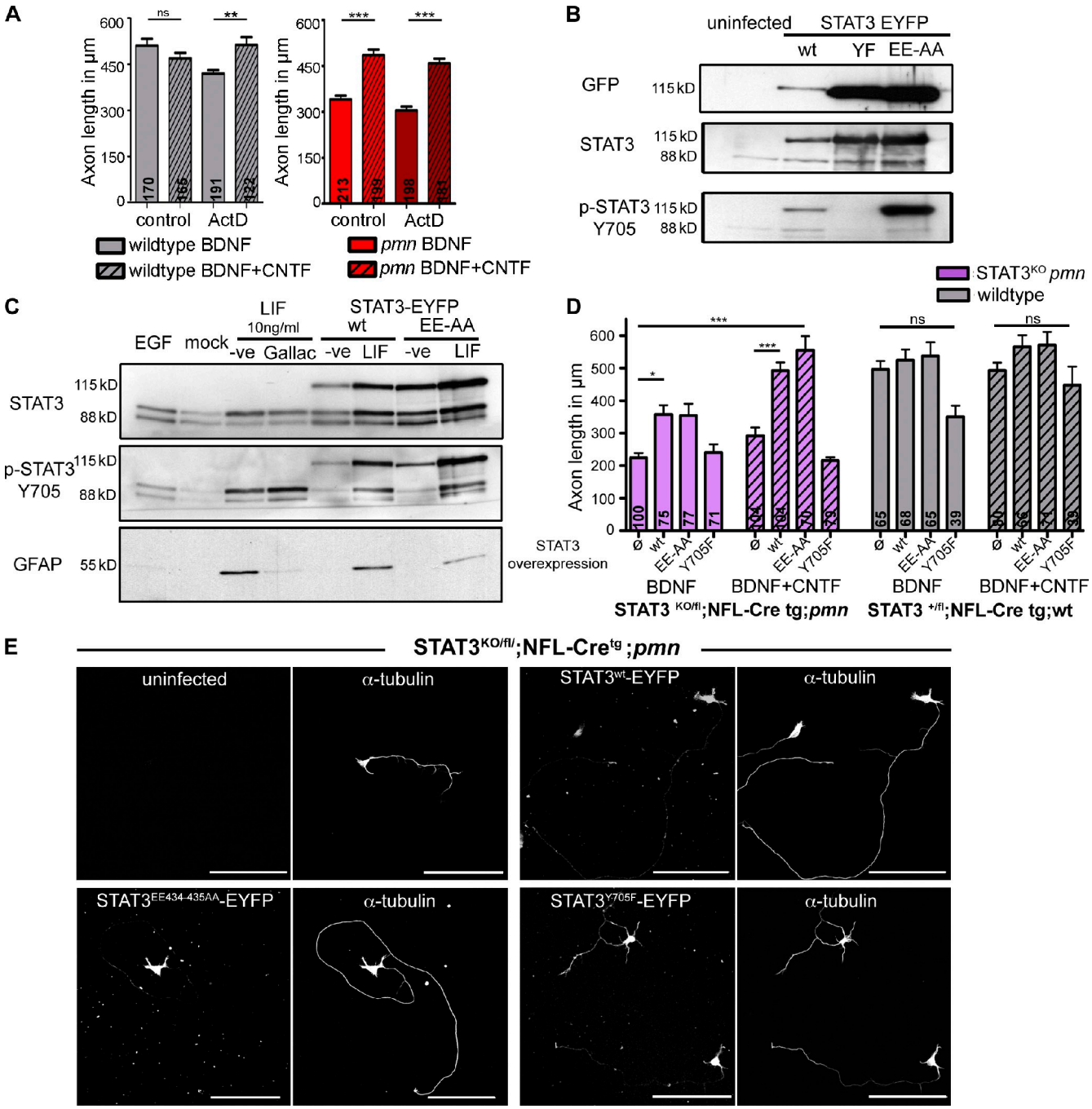

Figure 3. **Transcription-independent activity of STAT3 mediates axon growth in *pmn* mutant motoneurons.** (A) Axon length of wild-type and *pmn* mutant motoneurons in control or 5 nM actinomycin D–treated cultures after 5 DIV. Actinomycin D (ActD) was applied at 4 DIV for 24 h. Numbers in bars indicate numbers of cells analyzed. $n = 3$ independent experiments. Statistical analysis: **, $P < 0.01$; ***, $P < 0.001$; ANOVA with Bonferroni posthoc test. (B) Lentiviral overexpression of STAT3^{wt}-EYFP, STAT3$^{EE434–435AA}$-EYFP, and STAT3^{Y705F}-EYFP in primary motoneurons. Wild-type and EE434–435AA mutant STAT3 can be activated at tyrosine 705 but not the STAT3^{Y705F}-EYFP mutant. (C) LIF-induced GFAP induction in neural stem cells was reduced by STAT3$^{EE434–435AA}$-EYFP and 10 µM galiellalactone (Gallac), indicating that mutant STAT3$^{EE434–435AA}$-EYFP represses transcription of its target genes. (D) STAT3 phosphorylation, but not its transcriptional activity, is required for CNTF-mediated axon growth in *pmn* mutant motoneurons. Overexpression of STAT3$^{EE434–435AA}$-EYFP mutant in STAT3-KO;*pmn* mutant motoneurons completely rescues axon growth upon CNTF application in contrast to STAT3^{Y705F}-EYFP mutant. Ø represents uninfected, and WT, EE-AA, and Y705F represent lentiviral overexpression of STAT3^{WT}-EYFP, STAT3$^{EE434–435AA}$-EYFP, and STAT3^{Y705F}-EYFP, respectively. Numbers in bars indicate numbers of cells analyzed. $n = 3$ independent experiments. Statistical analysis: *, $P < 0.05$; ***, $P < 0.001$; ANOVA with Kruskal-Wallis with Dunn's multiple comparison test. (E) Representative images of STAT3-KO;*pmn* mutant motoneurons overexpressing STAT3^{wt}-EYFP, STAT3$^{EE434–435AA}$-EYFP, and STAT3^{Y705F}-EYFP and cultured with BDNF and CNTF. Bars, 100 µm. −ve, negative; wt, wild type. Data shown represent means ± SEM.

immunoprecipitated from motoneurons overexpressing STAT3^{wt}-EYFP and STAT3^{Y705F}-EYFP and then tested for STAT3 interaction. Stathmin interaction with STAT3^{Y705F}-EYFP was reduced when compared with STAT3^{wt}-EYFP, indicating that phosphorylation of STAT3 at Y705 by CNTF is required for binding of stathmin to STAT3 (Fig. 4 D).

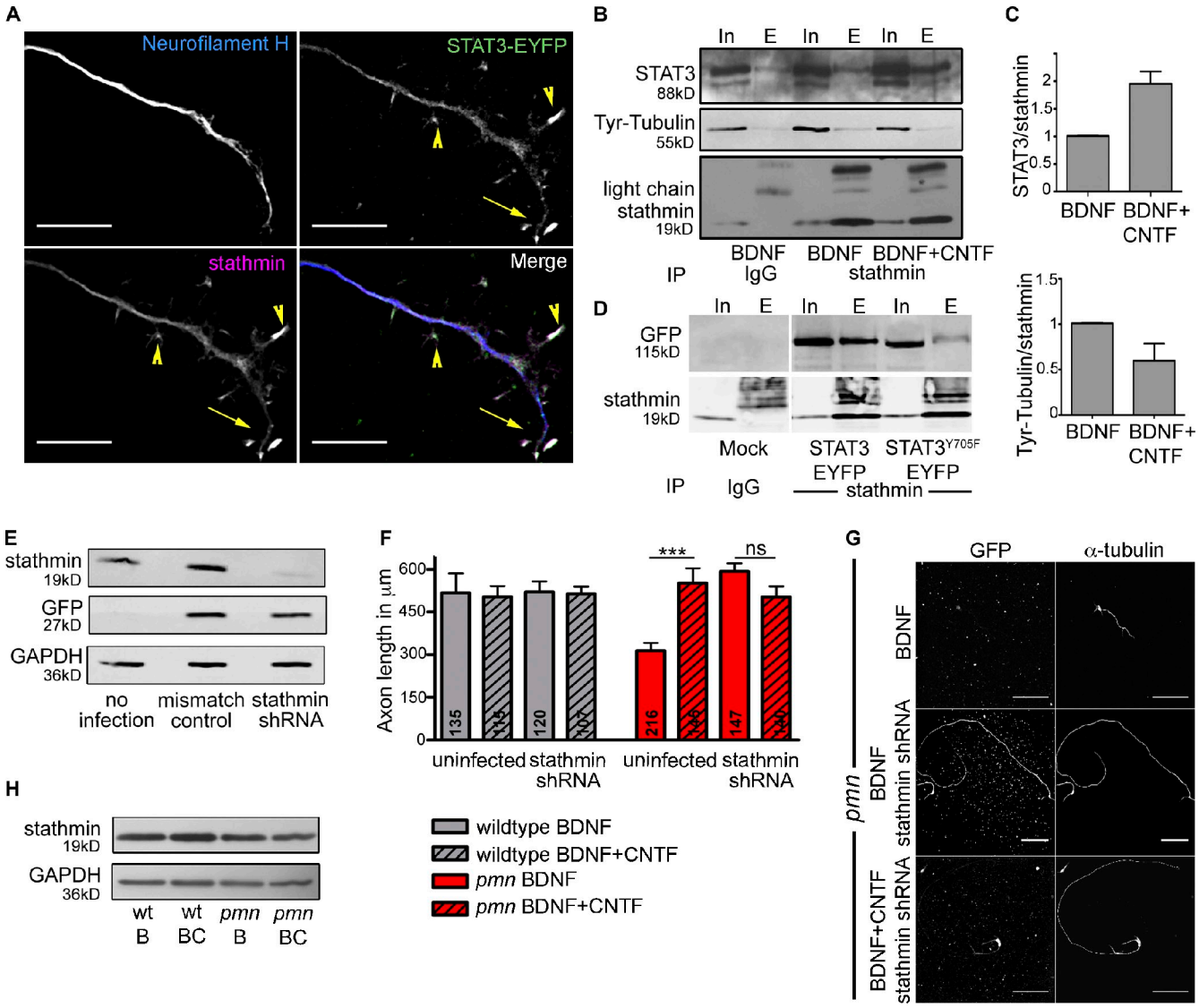

Figure 4. **Stathmin knockdown rescues axonal pathology in *pmn* mutant motoneurons.** (A) Colocalization of STAT3-EYFP and stathmin in cultured motoneurons. Both proteins are colocalized and enriched in branch points (arrowheads) and growth cones (arrows). Bars, 10 µm. (B) Immunoprecipitation of stathmin from motoneurons cultured for 5 DIV. Western blot analysis after immunoprecipitation shows that STAT3 interaction with stathmin is enhanced after CNTF application. (first and second lanes) Input (In) and eluate (E) from IgG control; (third and fourth lanes) input and eluate from motoneurons cultured with BDNF; (fifth and sixth lanes) input and eluate from motoneurons cultured with BDNF and pulsed with CNTF for 30 min on day 5. (C) Quantification of Western blot signals shows a twofold increase in the STAT3–stathmin interaction and reduced stathmin–tyrosinated (Tyr) tubulin interaction after CNTF application; $n = 3$ independent experiments. (D) Immunoprecipitation experiments of stathmin with wild-type and dominant-negative STAT3 (STAT3^{Y705F}-EYFP). Subsequent Western blot analysis shows loss of STAT3–stathmin interaction when phosphorylation at Y705 is abolished. White line indicates that intervening lanes have been spliced out. (E) Western blot analysis of protein extracts from cultured primary motoneurons after lentiviral stathmin knockdown. (F) Axon length is restored in *pmn* mutant motoneurons after lentiviral stathmin knockdown. Wild-type and *pmn* mutant motoneurons were cultured for 5 DIV. Stathmin knockdown rescues axon length in *pmn* mutant motoneurons. CNTF application did not induce additional axon growth in motoneurons with stathmin knockdown. Numbers in bars indicate number of cells measured. $n = 3$ independent experiments. ***, $P < 0.001$; Kruskal-Wallis with Dunn's multiple comparison test. (G) Representative images of *pmn* mutant motoneurons after lentiviral stathmin knockdown. Cells were labeled with GFP and α-tubulin (Cy-3) antibodies. Bars, 100 µm. (H) CNTF application does not alter stathmin protein level in primary motoneurons of wild-type and *pmn* mutant mice. BDNF and CNTF are indicated by B and C, respectively. IP, immunoprecipitation; wt, wild type. Error bars represent means ± SEM.

The release of α/β-tubulin heterodimers from inactivated stathmin could increase the availability of α/β-tubulin heterodimers for polymerization and thus lead to enhanced axon elongation in CNTF-treated *pmn* mutant motoneurons. To test this hypothesis, we generated a short hairpin RNA (shRNA) lentivirus for knockdown of stathmin. Using this lentivirus, stathmin levels decreased to <20% of control or control mismatch virus-treated cultures (Fig. 4 E). As expected, axon growth in *pmn* mutant motoneurons recovered to wild-type levels after stathmin knockdown (Figs. 4, F and G; and S5 B). CNTF addition did not lead to any further increase in axon growth, indicating that stathmin inhibition is the major pathway in which CNTF rescues axon growth in *pmn* mutant motoneurons. Interestingly, wild-type motoneurons did not show any enhanced axon elongation when treated with the stathmin shRNA virus (Fig. 4, F and H), and this was not caused by altered expression of stathmin

in wild-type versus *pmn* mutant motoneurons (Fig. 4 H). This observation indicates that local effects of STAT3 in the axon, involving stathmin, mediate the rescue effects of CNTF observed in *pmn* mutant motoneurons.

CNTF enhances MT stability in cultured motoneurons

Based on the finding that the interaction of stathmin with tyrosinated tubulin was reduced, we then tested MT dynamics in wild-type and *pmn* mutant motoneurons. Tyrosination of MTs has been shown as a characteristic feature of highly dynamic MTs, i.e., the MTs close to a moving growth cone (Witte et al., 2008). In contrast, acetylation occurs predominantly in stable, long-living MTs. Confirming a previous study with other neuronal cell types (Witte et al., 2008), we found acetylated tubulin in all parts of the axon but relatively excluded from axonal growth cones and dendrites (Fig. 5 A), where most MTs are thought to be more stable than in distal parts. Tyrosinated tubulin was in all regions of the neuron, including regions close to the axonal growth cone and in dendrites (Fig. 5 A). Surprisingly, levels of tyrosinated tubulin were significantly increased in axons of *pmn* mutant motoneurons in comparison to wild-type motoneurons when cultured with BDNF (Fig. 5 B), indicating that there are more highly dynamic MTs in the *pmn* mutant motoneurons under conditions when axons are shorter and axonal transport is reduced. Addition of CNTF and stathmin knockdown (Fig. 5 B, right bar) significantly reduced the levels of tyrosinated tubulin (Fig. 5 B), indicating that CNTF influences the dynamics of MTs and stabilizes them, presumably by deactivating the MT-destabilizing activity of stathmin. The levels of acetylated stable MTs were not different in *pmn* and wild-type motoneurons and not affected by CNTF or by stathmin knockdown (Fig. 5 C). We then tested whether stabilization of MTs is sufficient to restore axon elongation in *pmn* motoneurons. For this experiment, *pmn* and wild-type motoneurons were cultured in the presence of 10 nM taxol for 5 DIV, an MT-stabilizing drug reported previously to promote axon elongation via stabilization of MTs at these concentrations (Witte et al., 2008). Taxol treatment promoted increased axon growth (Fig. 5, D and E) comparable with the axon length observed in *pmn* motoneurons that were cultured with CNTF.

CNTF enhances MT polymerization in cultured motoneurons

Previous investigations with isolated *pmn* mutant motoneurons showed that MT polymerization is impaired because of the mutation in the *Tbce* gene (Schaefer et al., 2007). To test whether CNTF could influence MT dynamics and polymerization, we assessed MT reassembly after nocodazole treatment (Schaefer et al., 2007). Wild-type and *pmn* mutant motoneurons were plated on coverslips, and 10 µM nocodazole was added for 6 h to completely depolymerize the MT network (Fig. 6 A). MT regrowth after nocodazole washout was observed within 5 min. The polymerized MTs were extracted and subsequently fixed with 2% PFA. Cells were stained with antibodies for γ- and α-tubulin to localize the MT-organizing center (MTOC) and polymerized MTs, respectively. Sholl analysis was performed with radius increments of 0.25 µm to quantify the extent of MT polymerization emanating from the MTOC (Fig. 6 B). *pmn* mutant motoneurons showed lower numbers of intersections when compared with wild-type motoneurons (Fig. 6 C), corresponding to lower rates of MT polymerization. Application of CNTF significantly increased MT formation in *pmn* mutant motoneurons (Fig. 6 D). Also the mean length of MTs was lower when compared with wild-type motoneurons, and this was restored after CNTF application (Fig. 6 E). STAT3 deficiency abolished the effect of CNTF on the elongation of MTs in motoneurons (Fig. 6 F). Interestingly, CNTF treatment also enhanced MT reassembly in wild-type motoneurons (Fig. 6 G).

Discussion

Here, we show that CNTF, in contrast to BDNF or GDNF, stabilizes the axonal cytoskeleton of motoneurons by activation of STAT3. STAT3 stimulates MT regrowth and rescues MT destabilization in *pmn* mutant motoneurons that suffer from a mutation in the *Tbce* gene, coding for a chaperone that interacts with α-tubulin and stimulates the formation of α/β-tubulin dimers. The rescue effect of activated STAT3 involves stathmin, an 18-kD MT-interacting protein that binds α/β-tubulin heterodimers (Ng et al., 2006), thus reducing their availability for the assembly of MTs.

Neurotrophic factors from several gene families, including BDNF, GDNF, and CNTF, have originally been identified as potent survival factors for embryonic motoneurons (Sendtner et al., 1996). Similarly, these factors rescue motoneuron cell bodies after nerve lesion at early stages after birth (Sendtner et al., 1990, 1992). It remained open from these studies whether the requirements of adult neurons for survival are similar and whether the maintenance of axons and neuromuscular endplates depends on the same signals and signaling cascades as the maintenance of cell bodies during embryonic development and early postnatal stages. The observation that GDNF and CNTF differ in their capacity to prolong survival in mouse models of motoneuron disease, in particular the *pmn* mutant mouse (Sendtner et al., 1992; Sagot et al., 1996) that suffers from a mutation in the *Tbce* gene (Bommel et al., 2002; Martin et al., 2002)—despite similar survival effects on motoneuron cell bodies—indicates that signaling pathways for axon and synapse maintenance are different from those that support survival. Furthermore, cell type–specific depletion of STAT3 in motoneurons of embryonic mice does not influence survival of developing motoneurons (Schweizer et al., 2002). In the adult, STAT3 is necessary for survival (Schweizer et al., 2002) and axon regeneration (Bareyre et al., 2011). From these previous studies, it remained open whether STAT3 promotes axon regeneration via transcriptional effects in the nucleus, such as up-regulated expression of bcl-xl or reg-2 (Nishimune et al., 2000; Schweizer et al., 2002; Ben-Yaakov et al., 2012) or local effects in axons that directly modify the cytoskeleton and thus axon stability and regeneration. Neither inhibition of transcription nor overexpression of a DNA binding–deficient STAT3 abolishes the effects of CNTF on axon growth in *pmn* mutant motoneurons, and most of the axonal STAT3 remains local in axons and is not

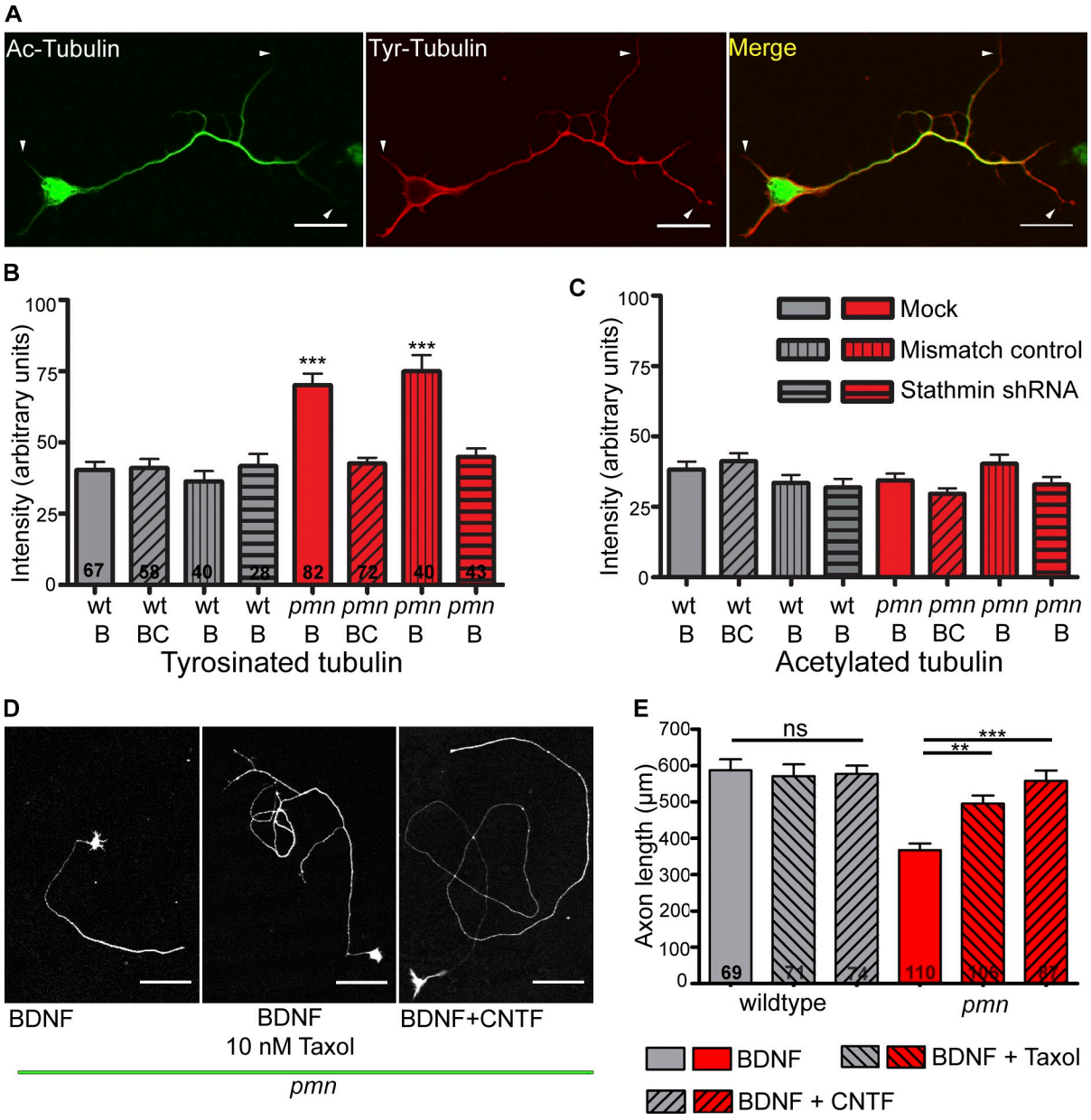

Figure 5. **MT stability is altered in *pmn* mutant motoneurons.** (A) Wild-type motoneuron stained with antibodies against acetylated and tyrosinated α-tubulin. Acetylated (Ac) tubulin (Cy2) labels stabilized MTs and is enriched in the axons but relatively excluded from dendrites and axonal growth cones (arrowheads). Tyrosinated (Tyr) tubulin (Cy3) labels dynamic and unstable MTs, including those in dendrites and axonal tips as shown by arrowheads. Bars, 20 µm. (B and C) Levels of tyrosinated and acetylated tubulin in *pmn* mutant motoneurons. (B) Levels of tyrosinated tubulin were increased in *pmn* mutant motoneurons when compared with wild-type motoneurons. 10 ng/ml CNTF treatment or stathmin knockdown in *pmn* mutant motoneurons reduced tyrosinated tubulin levels to wild-type levels. (C) Levels of acetylated tubulin were unchanged under conditions investigated. Numbers in bars indicate number of cells analyzed. BDNF and CNTF are indicated by B and C, respectively. Statistical analysis: ***, $P < 0.001$; ANOVA with Bonferroni posthoc test. (D) Representative pictures of *pmn* mutant motoneurons cultured with BDNF, 10 nM taxol, and BDNF and CNTF showing increased axon length upon stabilization of MTs. Bars, 100 µm. (E) Stabilization of MTs in *pmn* mutant motoneurons in the presence of 10 nM taxol increased axon length in *pmn* motoneurons to wild-type levels. Numbers in bars represent cells measured. Statistical analysis: ***, $P < 0.001$; ANOVA with Bonferroni posthoc test. wt, wild type. Error bars shown represent means ± SEM from three independent experiments.

retrogradely transported upon CNTF treatment, indicating that local signaling pathways could be involved in STAT3 effects on axon stability and maintenance.

Stabilization of MTs by taxol has a major effect on axon regeneration after spinal cord injury (Hellal et al., 2011). It increases total polymerized tubulin and decreases tyrosinated tubulin after axonal lesion and thus promotes regeneration of dorsal root sensory nerve fibers after spinal cord lesion (Hellal et al., 2011). This finding indicates that local regulatory mechanisms modifying the turnover and stability of MTs could play a central role under conditions when axons regenerate and possibly also under conditions of synapse pruning and axonal degeneration, such as in motoneuron disease. Stathmin, also named Op18 (oncoprotein-18) is a member of a family of MT interaction proteins that also includes the SCG10 (superior cervical ganglion protein 10), the SCLIP (SCG10-like protein),

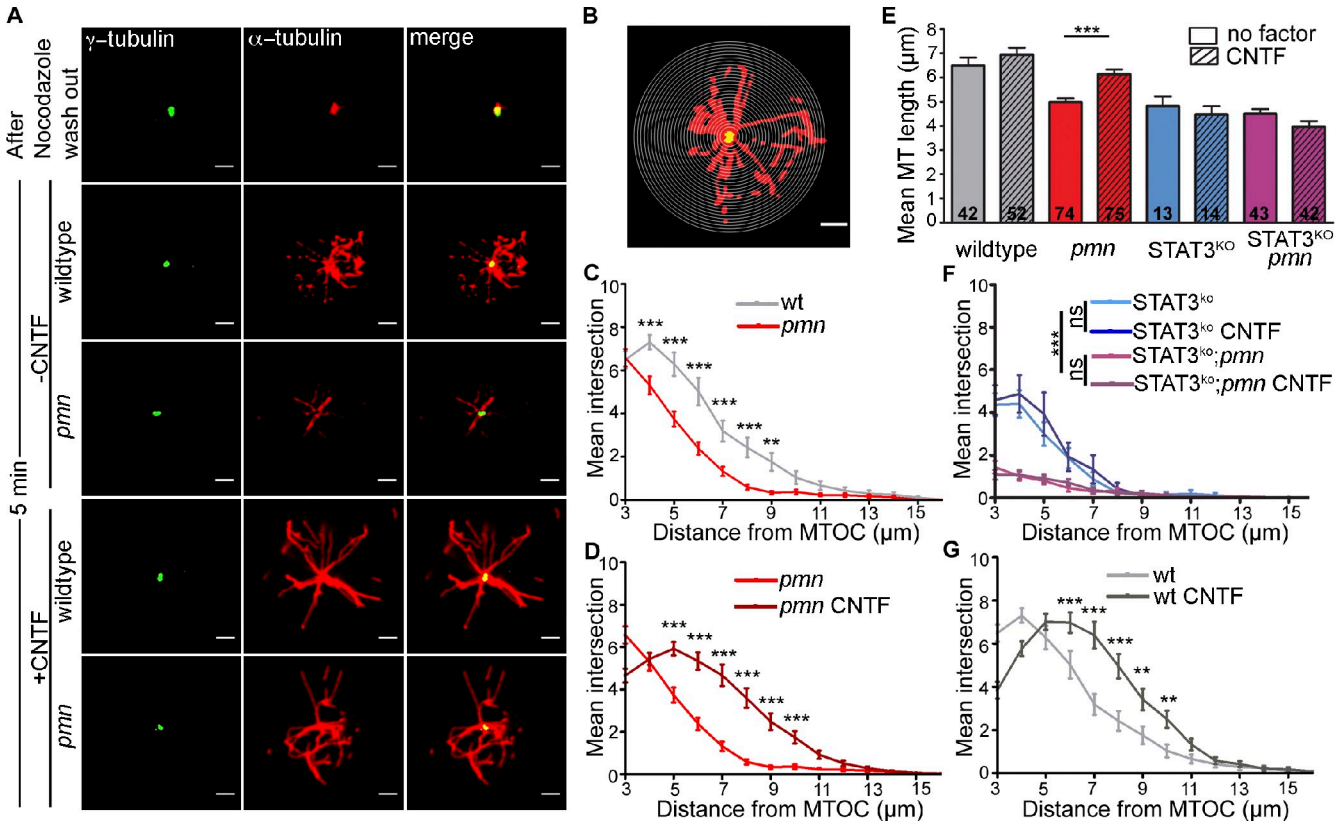

Figure 6. **CNTF enhances MT regrowth in cultured motoneurons.** (A) MTs were depolymerized with nocodazole, and MT regrowth was analyzed at 5 min after CNTF application in cultured wild-type and *pmn* mutant motoneurons. The centrosome is labeled with γ-tubulin (Cy2), and MTs were labeled with α-tubulin (Cy3). Bars, 2 µm. (B) Representative image from Sholl analysis performed on primary motoneurons with 0.25-µm step concentric circles. Bar, 2 µm. (C, D, F, and G) Graphs obtained from Sholl analysis depicting number of intersections on y axis and distance from MTOC on the x axis. (C) Comparison of MT regrowth between *pmn* mutant and wild-type motoneurons. (D) CNTF enhances MT regrowth in *pmn* mutant motoneurons. (E) Graphical representation of mean length of polymerized MTs formed in wild-type and *pmn* mutant motoneurons with and without CNTF and in $STAT3^{fl/KO}$;$NFL\text{-}Cre^{tg}$ motoneurons. Numbers in bars represent the number of analyzed motoneurons. Error bars shown represent means ± SEM from four independent experiments. Statistical analysis: ***, $P < 0.001$; ANOVA with Bonferroni posthoc test. (F) CNTF-mediated MT regrowth was abolished in $STAT3^{fl/KO}$;$NFL\text{-}Cre^{tg}$ and $STAT3^{fl/KO}$;$NFL\text{-}Cre^{tg}$;*pmn* mutant motoneurons. (G) CNTF enhances MT regrowth in wild-type motoneurons. Statistical analysis: **, $P < 0.01$; ***, $P < 0.001$; two-way ANOVA with Bonferroni posthoc test. wt, wild type.

and RB3, all sharing a conserved tubulin-binding domain in their C terminus (Charbaut et al., 2001). There are two mechanisms by which stathmin and related family members modulate MT turnover and stability. They directly induce catastrophe-promoting MT depolymerization, and they sequester tubulin heterodimers and thus could have an indirect effect on polymerization of new MTs. Our observation that CNTF restores regrowth of MTs after nocodazole treatment suggests that the second mechanism could play a central role, in particular under the specific condition in *pmn* mice in which a mutation of TBCE leads to reduced assembly of tubulin heterodimers. The $p\text{-}STAT3^{Y705}$–stathmin interaction has been observed upon cytokine stimulation in several cell types, including T lymphocytes (Verma et al., 2009) and various cell lines (Ng et al., 2006). These studies showed that STAT3, when overexpressed together with stathmin, binds to its C terminus, the same region that also interacts with tubulin heterodimers (Ng et al., 2006). Our data suggest that this interaction plays a major role for the maintenance of motor axons in the *pmn* mutant mouse, a model for motoneuron disease. Depletion of STAT3 by genetic ablation abolishes the rescue effect of CNTF on axon elongation in *pmn* mutant motoneurons. MT regrowth in isolated motoneurons after nocodazole treatment also showed that the effect of CNTF on MT polymerization depends on STAT3. shRNA-mediated knockdown of stathmin has similar effects as STAT3 activation. This raises the question why other members of the stathmin family could not recue. SCG10, SCLIP, and RB3 are palmitoylated at domain A and thus targeted to Golgi- and vesicle-like structures, in contrast to stathmin, which is mainly found in the cytosol (Chauvin et al., 2008). This indicates that stathmin could be more abundant in axons and axon terminals in comparison to SCLIP and the other members of this family. Indeed, SCLIP has been shown to be a major regulator of dendrite growth in Purkinje cells (Poulain et al., 2008), indicating that differences in subcellular distribution and binding to the Golgi compartment could contribute to such differential effects.

A recent study has shown that TBCE and the related TBCE-like protein can also cause degradation of α/β-tubulin heterodimers, in particular when these proteins are overexpressed (Sellin et al., 2008), and that stathmin counteracts the tubulin-disrupting activity of these proteins. Stathmin depletion thus shifts the balance between preservation of α/β-tubulin

heterodimers to degradation, and this could explain why stathmin depletion is less active in promoting axon growth in wild-type motoneurons than in *pmn* mutant motoneurons in which TBCE levels are reduced.

CNTF reduces the levels of tyrosinated MTs in distal parts of axons in *pmn* mutant motoneurons and thus resembles the effects observed with taxol after axonal lesion (Hellal et al., 2011). The stabilization of MTs in the distal axons could play a major effect for the improved clinical phenotype in CNTF-treated mice (Sendtner et al., 1992), and it will be interesting to know whether the effect of CNTF on pruning of neuromuscular endplates (Pun et al., 2006) depends on this effect on MTs. Proximal axons are generally more stable, and this correlates with acetylation of MTs. Interestingly, CNTF effects on MT acetylation were low, although the number of proximal MTs was reduced. This indicates that the dynamics of MTs that is higher in distal axons is influenced by CNTF via STAT3–stathmin signaling.

Previous studies have shown that stathmin and other members of this family are inactivated by phosphorylation. These proteins are substrates of JNK kinases, and the effects of JNK on the MT cytoskeleton seem to be mediated by this interaction (Tararuk et al., 2006; Ng et al., 2011). Inactivation of stathmin has also been shown to occur via phosphorylation in a Rac-dependent manner via DOCK7 for axon initiation in developing neurons (Watabe-Uchida et al., 2006). Once axons are initiated, a dramatic influx of tubulin heterodimers into the nascent axon contributes to axon elongation (Yu et al., 2001).

The phosphorylation of stathmin, which inactivates this protein in its MT-binding activity in a similar way as interaction with STAT3, could in principle occur in two modes that need to be distinguished. For example, BDNF stimulates transcription of MKP-1, a phosphatase that dephosphorylates JNK in developing neurons and thus leads to a global reduction of stathmin phosphorylation in developing neurons, thus destabilizing MTs as a prerequisite for neurite branching (Jeanneteau et al., 2010). On the other side, local signaling, via transmembrane proteins that are only present in specific subdomains of neurons could locally influence the cytoskeleton. For example, ephrin B and laminin alter phosphorylation of SCG10 (Suh et al., 2004) and thus modulate growth cone protrusion in the context of axon guidance. Similar effects were observed downstream of Kidins220/ARMS, which associates with ephrins and neurotrophin receptors (Higuero et al., 2010). Stabilization of axon terminals at synapses and axons thus could represent a specific target for local signals at neuromuscular junctions and motor axons that stabilize neuromuscular endplates and distal axons. In line with this hypothesis, increase in acetylated tubulin, which marks stable MTs in enlarged axonal growth cones, was identified as a specific effect of agrin signaling in cultured hippocampal neurons (Bergstrom et al., 2007). In other mouse models of motoneuron disease, i.e., SOD-1 mutant mice, local application of CNTF, but not GDNF, significantly delays the depletion of synaptic vesicles from presynaptic zones during the process of pruning of neuromuscular endplates (Pun et al., 2006). This difference suggests that similar mechanisms could play a role for axonal maintenance and synaptic vesicle stalling. Collectively, these findings indicate that local signals that stabilize MTs also stabilize and maintain neuromuscular endplates and axonal projections in postnatal motoneurons. Thus, inhibition of stathmin could be a target for therapy in neurodegenerative disorders, such as motoneuron disease, in which destabilization of synapses and distal axons reflect a major step in the pathophysiological cascade.

Materials and methods

Animals

All mouse lines used in this study were maintained on a Naval Medical Research Institute (NMRI) genetic background. *pmn* mutant mice were maintained as a heterozygote line by backcrossing with wild-type NMRI mice, and homozygous *pmn* mutant embryos were obtained by crossing heterozygous mice. Conditional STAT3 knockout (KO) was achieved by crossing a mouse line homozygously transgenic for NFL-Cre and carrying a STAT3-null allele ($STAT3^{KO/wt}$;$NFL\text{-}Cre^{tg/tg}$) with mice homozygous for loxP-flanked STAT3 ($STAT3^{fl/fl}$) as previously described (Schweizer et al., 2002).

To obtain the STAT3-deficient *pmn* mutant ($STAT3^{fl/KO}$;$NFL\text{-}Cre^{tg}$;$pmn^{-/-}$) embryos for motoneuron culture experiments, $STAT3^{KO/wt}$;$NFL\text{-}Cre^{tg/tg}$ and $STAT3^{fl/fl}$ mice were crossed with $pmn^{+/-}$ mice to generate $STAT3^{KO/wt}$;$NFL\text{-}Cre^{tg}$;$pmn^{+/-}$ and $STAT3^{fl/fl}$;$pmn^{+/-}$ animals. These two lines served as the parental generation for litters that contain STAT3-deficient *pmn* mutant embryos.

Antibodies

Antibodies against MAP2 (clone AP-20; M1406), tau (T-6402), acetylated α-tubulin (clone 6-11b-1; T7451), and α-tubulin (clone B-5-1-2; T5168) were purchased from Sigma-Aldrich. Antibodies against tyrosinated α-tubulin (clone YL1/2; ab6160), stathmin (clone EP1573Y; ab52630), histone 3 (ab1791), and chicken anti-GFP (ab13970) were obtained from Abcam. Antibodies against STAT3 and p-$STAT3^{Y705}$ were supplied from Cell Signaling Technology, anti–glyceraldehyde 3-phosphate dehydrogenase (GAPDH) was obtained from EMD Millipore, rabbit anti-GFP (sc 8334) and rabbit anti-TrkB (sc 8316) were obtained from Santa Cruz Biotechnology, Inc., and chicken anti-NFL heavy (AB5539) was purchased from EMD Millipore.

Primary motoneuron culture

Lumbar spinal motoneurons were isolated from E13.5 mouse embryos as previously described (Wiese et al., 2010) with minor modifications. The spinal cord was dissected, and the ventrolateral parts of the lumbar segments were collected in HBSS. The tissues were trypsinized (0.1%) for 15 min at 37°C, and motoneurons were enriched by immunopanning using the p75NTR antibody. The p75NTR antibody, clone MLR2 (a gift from R. Rush, Flinders University, Adelaide, Australia; Rogers et al., 2006), also commercially available through Biosensis (catalog no. M-009-100) and Abcam (catalog no. ab61425), was used at 5 ng/ml to precoat Nunclon Δ surface culture dishes for immunopanning. Enriched motoneurons were plated on glass coverslips (Marienfeld) from a pretested batch in culture dishes (Greiner Bio-One) or µ-dishes (Ibidi) precoated with polyornithine and laminin-111 (catalog no. 23017–015, lot no. 1347084; Invitrogen). The same batch of laminin was used for all experiments with cultured motoneurons shown in this paper. Motoneurons were grown at 37°C and 5% CO_2 in neurobasal medium (Invitrogen) containing 500 µM GlutaMAX (Invitrogen), 2% horse serum (Linaris), 2% B27 supplement (Invitrogen), and neurotrophic factors BDNF (1–5 ng/ml), CNTF (1 or 10 ng/ml), or GDNF (5 ng/ml) as indicated. 50% of culture medium was exchanged on day 1 and then every second day. For axon length measurement, motoneurons were plated at a density of 2,000 cells/cm^2, and for electron microscopy and live imaging, they were plated at densities of 5,000 or 10,000 cells/cm^2.

Cortical precursor cell culture

Cortical precursor cell cultures were prepared as previously described (Götz et al., 2005). In brief, embryonic forebrains were dissected at E12, trypsinized (0.1%), and cultured as neurospheres in neurobasal medium containing 500 µM GlutaMAX, 50 U/ml penicillin G sodium, 50 U/ml streptomycin sulfate (Invitrogen), 2% B27 supplement, basic FGF (bFGF), and EGF (Cell Concepts) at final concentrations of 20 ng/ml each. The cells were grown at 37°C in a 5% CO_2 humidified atmosphere. Cells were dissociated cultured on poly-DL-ornithine– and laminin1-coated 12-well cell culture dishes at a density of 100,000 cells per well in culture medium with

bFGF and EGF. Appropriate lentiviral infections were performed before plating of the cells. bFGF and EGF were withdrawn after 48 h, and cells were then treated with 10 ng/ml LIF for 24 h.

Electron microscopy

Primary motoneurons (E13.5) were cultured for 7 DIV and fixed for 5 min at 37°C with 2% glutaraldehyde in 0.05 M phosphate buffer, pH 6.8. Cells were then treated with osmium tetroxide, subjected to series of alcohol dehydration, and embedded in Epon resin. After polymerization, the resins were stained with methylene blue. Ultrathin sections of 80 nm were prepared, transferred to Formvar-coated nickel grids, and contrasted with uranyl acetate and lead citrate. Electron micrographs were obtained with a transmission electron microscope (LEO 912 AB; Carl Zeiss). MT density in longitudinal axonal sections was assessed following a method described previously (Daniels, 1973). 12 regularly spaced (173-nm distance) parallel lines perpendicular to the long axis of the axon were superimposed upon micrographs taken from proximal parts of the axons (within ∼50 µm of the cell body), distal parts (less than ∼100 µm proximal to the axon tip), and intermediate parts (in between). For each line, the distance across the axon and the number of MT intersections were recorded, and the mean number of MT intersections was divided by the mean distance across the axon to yield an estimate of MT density (given as intersections per 500 nm).

Lentiviral production

STAT3-EYFP-N1 expression vector was provided by F. Horn (University Hospital, Leipzig, Germany; Kretzschmar et al., 2004). Dominant-negative $STAT3^{Y705F}$-EYFP and $STAT3^{EE434–435AA}$-EYFP were generated with the help of a site-directed mutagenesis kit (QuikChange; Agilent Technologies) using the mutagenesis primers as follows: $STAT3^{Y705F}$ forward, 5′-GTAGTGCTGCCCGTTCCTGAAGACCAAG-3′; $STAT3^{Y705F}$ reverse, 5′-CTTGGTCTTCAGGAACGGGGCAGCACTAC-3′; $STAT3^{EE434–435AA}$ forward, 5′-CCTCCTTGATCGTGACCGCGGCGCTGCACCTGATCACC-3′; and $STAT3^{EE434–435AA}$ reverse, 5′-GGTGATCAGGTGCAGCGCCGCGGTCACGATCAAGGAGG-3′. STAT3-EYFP, $STAT3^{EE434–435AA}$-EYFP, and $STAT3^{Y705F}$-EYFP were subcloned into the FUGW (Lois et al., 2002) vector through the Nhe1–Not1 site. The HEK293T cell line was used to generate viruses as described previously (Lois et al., 2002). HEK293T cells were transfected with packaging vector pCMVΔR8.9 s, generation envelope vector pVSVG, and expression plasmids FUGW-STAT3-EYFP, FUGW-$STAT3^{Y705F}$-EYFP, or FUGW using Lipofectamine 2000 (Invitrogen). Supernatants were collected and concentrated by ultracentrifugation. Lentiviruses were aliquoted and stored at −80°C until use.

The knockdown vector for stathmin was generated cloning stathmin shRNA sequence (5′-TCGAGAAAAAAGGGGAGAAACTGAAAGTGTTCTCTTGAAACACTTTCAGTTTCTCCCCA-3′) and mismatch shRNA (5′-GAAAAAAGGTTAGAAACTTAAAGTGTTCTCTTGAAACACTTTAAGTTTCTAACCA-3′) into pLL3.7 Lentilox vector. Lentiviruses were generated as described previously (Bender et al., 2007).

Immunocytochemistry

Cells were cultured for either 5 or 7 d depending on the experiment, washed once with PBS to remove serum components, and fixed with 4% PFA for 20 min at room temperature. Cells were washed three times with PBS and blocked for 30 min at room temperature with blocking buffer containing 15% goat serum and 0.3% Triton X-100 in TBST (TBS-Tween). Primary antibodies diluted in blocking buffer were then added and incubated overnight at 4°C. Cells were then washed three times with TBST, and corresponding secondary antibodies coupled with fluorophores were added and incubated at room temperature for 1 h. Coverslips were washed and mounted on glass slides with Mowiol or aqua polymount. Imaging was performed with the confocal microscopy (SP2; Leica) with a 40× oil immersion objective, NA 1.25, and 8-bit mode. Axon length and intensity measurements were performed using the LCS AF Lite software (Leica). The experimentators were blind with respect to the genotypes for *pmn*, STAT3, and NLF-Cre^{tg}, and the results from genotyping were only revealed after the analysis of axon length measurements and quantification of axonal swellings had been completed. For quantification of axonal swellings (Bommel et al., 2002), fixed motoneurons were stained with MAP2 and tau (Wiese et al., 2010). Axonal swellings imposed as local varicosities in axons containing disorganized filaments (Bommel et al., 2002) and deformed mitochondria (see also Fig. 1 D, electron micrographs). The number of axonal swellings was determined from digital photographs of MAP2/tau-stained motoneurons, and a ratio of the number of swellings per length of the total axon was recorded. Data in Fig. 1 C show the calculated ratio of the number of swellings/1,000 µm.

Nuclear fractionation

Primary motoneurons (∼250,000 cells, derived from four litters and ∼30 mouse embryos) were cultured for 4 DIV with culture medium containing 5 ng/ml BDNF. Cells were washed three times with neurobasal medium to remove serum components and further cultured overnight in serum-free medium with BDNF. 10 ng/ml CNTF was applied for 5, 15, and 30 min. In parallel, CNTF was applied for 5 d continuously to one culture. Cells were washed once with PBS (PAA Laboratories) and lysed with the nuclear fractionation buffer containing 50 mM Tris-HCl, pH 7.4, 150 mM NaCl, 1% NP-40, 2 mM EDTA, pH 8.0, protease inhibitor (Roche), 10 mM sodium pyrophosphate, 2 mM sodium orthovanadate, 1 mM sodium fluoride, and 1 mM okadaic acid for 10 min at 4°C. Cells were scrapped off and centrifuged at 1,000 *g* for 15 min at 4°C. The supernatant was removed and used as a cytoplasmic fraction. The pellet was washed once with PBS and centrifuged again at 20,000 *g* for 10 min at 4°C. The pellet was used as a nuclear fraction. Cytoplasmic and nuclear fractions were controlled using GAPDH (clone 6C5; CB 1001) and histone 3 antibodies as respective markers.

Western blotting

Primary motoneurons were lysed with nuclear fractionation buffer or directly with Laemmli buffer (125 mM Tris, pH 6.8, 4% SDS, 10% β-mercaptoethanol, 20% glycerol, and 0.004% bromophenol blue) and boiled for 10 min at 99°C. Proteins were then subjected to SDS-PAGE, blotted onto nitrocellulose membrane, incubated with corresponding antibodies, and developed with either ECL or ECL Advance systems (GE Healthcare). Western blots were scanned and quantified by densitometry analysis with ImageJ (National Institutes of Health).

Immunoprecipitation

Primary motoneurons (approximately three million cells derived from ∼300 mouse embryos) were cultured for 5 DIV. Nuclear and cytoplasmic proteins were extracted as described in the Nuclear fractionation section. CNTF was applied for 30 min on day 5 before fractionation. Cell lysates from 5 ng/ml BDNF- and 10 ng/ml BDNF + CNTF–treated cultured motoneurons were incubated with 5 µl rabbit antistathmin antibody overnight at 4°C. IgG control was included by incubating the lysate with irrelevant rabbit anti-TrkB antibody. Protein G–agarose beads (Roche) were washed with PBS and equilibrated with lysis buffer. Protein lysate and antibody were incubated with equilibrated beads for 1 h under rotary agitation at 4°C. After incubation, supernatant was removed by centrifugation at 1,000 *g*, and beads were washed three times with lysis buffer. Proteins were eluted by boiling the beads with 2× Laemmli buffer. Immunoblotting was performed for STAT3, stathmin, tyrosinated tubulin, and GFP to confirm coimmunoprecipitation. Densitometry analysis was performed using ImageJ software to quantify band intensities.

MT regrowth

An established MT regrowth assay was performed in cultured motoneurons (Schaefer et al., 2007). In brief, motoneurons were plated on laminin1-coated coverslips, and 1 h after attachment, the cells were treated with 10 µM nocodazole and incubated for 6 h at 37°C to depolymerize the MT network. Cells were washed with neurobasal medium and treated with 10 ng/ml CNTF for 5 min. Cells were rinsed with MT-stabilizing buffer PHEM (60 mM Pipes, 25 mM Hepes, 10 mM EGTA, and 2 mM $MgCl_2$). Cells were extracted with 0.5% Triton X-100 and 10 µM paclitaxel (Sigma-Aldrich) in PHEM buffer for 3 min, which washes away the soluble tubulin fraction and retains polymerized tubulin. Cultures were fixed with equal volume of PHEM buffer containing 4% PFA. Cells were immunostained for γ-tubulin to label the centrosome and α-tubulin to label polymerized MTs. Images were acquired by confocal microscopy with 63× oil immersion objective, 4× magnification, and 1.4 NA. Images were loaded in one stack using McMaster Biophotonics Facility ImageJ and enhanced by background subtraction radius 50 filter median to reduce noise, and a threshold was set to all pictures. Sholl analysis was performed with ImageJ with steps of 0.25 µm.

The total length of MTs formed in each cell was calculated by determining the number of intersections crossed by MTs and multiplying this number with the corresponding distance from the MTOC. This analysis was performed starting from the periphery to the center. Individual MTs were only included once in this analysis when they crossed the most outer circle around the MTOC. Mean length was calculated by summing up the length of MTs obtained and divided by the total number of MTs measured: $\sum ((n_x - n_{x+1}) \times \Delta MTOC_x)/N$, in which n is the number of intersections, x is the circle of interest, $x + 1$ is the next outer circle, $\Delta MTOC_x$ is the distance from MTOC to the circle of interest, and N is the total number of MTs.

Live imaging of mitochondria

Mitochondria were stained with 0.2 µg/ml Rhodamine 123 (Invitrogen) or 100 nM MitoFluor red 594 (Invitrogen) in culture medium containing 10 nM β-mercaptoethanol. Motoneurons were incubated for 15 min at 37°C and 5% CO_2 in the presence of dye and subsequently washed three times with neurobasal medium. Imaging was performed using a microscope (Eclipse TE2000; Nikon) with a 60× Plan Apochromat, NA 1.4 immersion objective combined with Perfect Focus System (Nikon) and a top stage incubation chamber and objective heater (Tokai Hit). Mitochondrial dye was excited with a xenon arc lamp using a 470/22-nm or 556/20-nm band pass filter for Rhodamine 123 or MitoFluor red 594, respectively. Emission was filtered by a 512/630-nm dual-band filter through a 493/574-nm dual-band beam splitter and recorded with a charge-coupled device camera (iXon; Andor Technology). For quantification of mitochondrial movement, image sequences were analyzed using the ImageJ plugins manual tracking and multiple kymographs.

FRAP

Lentivirally transduced motoneurons expressing STAT3-EYFP fusion protein or EGFP under the human ubiquitin C promoter as a control were cultured for 6 DIV. FRAP experiments were performed with a confocal laser-scanning microscope (SP5; Leica) using LAS AF imaging software with FRAP wizard. Motoneurons grown on coverslips (see Primary motoneuron culture methods) were placed into an imaging chamber and perfused with prewarmed (37°C) carbogen-gased culture medium. Images were acquired in 12-bit mode with a 20× glycerol immersion objective, NA 0.7, and an optical zoom factor of 2.0. EGFP or EYFP were excited using a 488- or 514-nm laser line, respectively, with 80% initial power of a 2.5-mW krypton/argon laser. Imaging speed was set to 400 Hz with a resolution of 512 × 512 pixels. To avoid photobleaching during prebleach as well as postbleach acquisition, laser intensity was set to 6% for 488-nm or 15% for 514-nm laser line of the preset 80% power. To achieve maximal beaching during the bleaching phase, the laser beam was focused on the region of interest using the zoom-in mode (FRAP wizard; Leica) together with 100% laser intensity. Bleaching was achieved with 10 frames at one frame/0.662 s.

Imaging conditions were as follows: Application of 10 ng/ml CNTF was achieved by changing the perfusion supply from culture medium containing only 5 ng/ml BDNF to culture medium containing 10 ng/ml BDNF and 10 ng/ml CNTF. Motoneurons were incubated with factors for 30 min before the FRAP experiments and kept under continuous perfusion. To inhibit MT-based transport, motoneurons were transferred to the imaging chamber 15 min before imaging and perfused with prewarmed (37°C) carbogen-gased culture medium containing 10 µM nocodazole without or with CNTF. To block local translation, motoneurons were incubated at 37°C and 5% CO_2 in culture medium containing 100 µg/ml cycloheximide 1 h before FRAP experiments.

Data analysis

Intensity of fluorescence was read out from bleached areas proximal and distal within the bleached axonal segment. FRAP data were exported from LAS-AF imaging software (Leica) to Excel (2003; Microsoft). Fluorescence intensities in proximal and distal segments were background corrected and normalized as indicated: $F(norm,t) = (F_t - F_{t,\ background}) - (F0 - F_{background})/(F0 - F_{background})$, in which $F(norm,t)$ is the normalized fluorescence intensity at time point t, F_t is the fluorescence intensity at given time point t, $F_{t,\ background}$ is the background signal at time point t, F0 is mean fluorescence intensity of 10 consecutive images taken before bleaching, and $F_{background}$ is the background signal during the prebleach phase. Normalized and background-corrected FRAP data were exported to Prism 4 (GraphPad Software). Single experiments were fitted using one-phase decay function and least-square fit to obtain rate constants of different conditions.

For better visualization of the representative FRAP image in Fig. 2 D, images from the time-lapse image series were processed with the image enhancement plugin of ImageJ using the following settings: background subtraction radius = 50, filter to reduce noise = median, percentage saturation = 0.3, and γ value adjustment = 0.6. Subsequently, motoneuron topology was altered using the ImageJ plugin straighten for better representation of the montage shown in Fig. 2 D.

Actinomycin D treatment

Primary *pmn* mutant and corresponding wild-type motoneurons of the same litter were cultured with 5 ng/ml BDNF or 10 ng/ml BDNF and CNTF. Afterward, 4 DIV wild-type and *pmn* mutant motoneurons cultures were treated with actinomycin D (Sigma-Aldrich) at a final concentration of 5 nM. Actinomycin D–treated and control cultures were fixed 24 h later and stained for tyrosinated α-tubulin and MAP2 and subsequently imaged.

Statistical analysis

Statistical analyses were performed with the Prism 4 software. All data are expressed as means ± SEM. Student's *t* test was used to compare two groups and analysis of variance (ANOVA) test with Bonferroni posthoc test, or nonparametric Kruskal-Wallis test with Dunn's multiple comparison test was used if there were more than two groups. Two-way ANOVA was used to test for significant differences between two categories and two conditions.

Online supplemental material

Fig. S1 shows the survival of motoneurons with different neurotrophic factors. Fig. S2 shows the quantification of axon diameter and MT density in cultured wild-type and *pmn* mutant motoneurons. Fig. S3 shows that CNTF restores reduced anterograde mitochondrial transport in *pmn* mutant motoneurons. Fig. S4 shows survival of motoneurons on different concentrations of actinomycin D. Fig. S5 demonstrates that STAT3 colocalizes with stathmin in the cell body and dendrites of cultured motoneurons and the specific function of the shRNA against stathmin. Online supplemental material is available at http://www.jcb.org/cgi/content/full/jcb.201203109/DC1.

We would like to thank Katrin Walter and Regine Sendtner for excellent technical assistance in animal breeding, genotyping, and histology and Friedemann Horn for providing the STAT3-EYFP-N1 expression vector.

This work was supported by the Sobek-Stiftung, the Deutsche Forschungsgemeinschaft, Sonderforschungsbereich 581, Teilprojekt B4, the European Union through the FP7 program EUROMOTOR (no. 259867), and the Federal Ministry of Education and Research, Motoneuron Disease Network.

Author contributions: M. Sendtner, B.T. Selvaraj, and N. Frank designed the experiments and wrote the manuscript, and F.L.P. Bender and E. Asan contributed to the experiments.

Submitted: 20 March 2012
Accepted: 2 October 2012

References

Amayed, P., D. Pantaloni, and M.F. Carlier. 2002. The effect of stathmin phosphorylation on microtubule assembly depends on tubulin critical concentration. *J. Biol. Chem.* 277:22718–22724. http://dx.doi.org/10.1074/jbc.M111605200

Andersen, J. 2003. Defects in dynein linked to motor neuron degeneration in mice. *Sci. SAGE KE.* 2003:PE10. http://dx.doi.org/10.1126/sageke.2003.18.pe10

Bareyre, F.M., N. Garzorz, C. Lang, T. Misgeld, H. Büning, and M. Kerschensteiner. 2011. In vivo imaging reveals a phase-specific role of STAT3 during central and peripheral nervous system axon regeneration. *Proc. Natl. Acad. Sci. USA.* 108:6282–6287. http://dx.doi.org/10.1073/pnas.1015239108

Bender, F.L., M. Fischer, N. Funk, N. Orel, A. Rethwilm, and M. Sendtner. 2007. High-efficiency gene transfer into cultured embryonic motoneurons using recombinant lentiviruses. *Histochem. Cell Biol.* 127:439–448. http://dx.doi.org/10.1007/s00418-006-0247-5

Ben-Yaakov, K., S.Y. Dagan, Y. Segal-Ruder, O. Shalem, D. Vuppalanchi, D.E. Willis, D. Yudin, I. Rishal, F. Rother, M. Bader, et al. 2012. Axonal transcription factors signal retrogradely in lesioned peripheral nerve. *EMBO J.* 31:1350–1363. http://dx.doi.org/10.1038/emboj.2011.494

Bergstrom, R.A., R.C. Sinjoanu, and A. Ferreira. 2007. Agrin induced morphological and structural changes in growth cones of cultured hippocampal neurons. *Neuroscience*. 149:527–536. http://dx.doi.org/10.1016/j.neuroscience.2007.08.017

Bommel, H., G. Xie, W. Rossoll, S. Wiese, S. Jablonka, T. Boehm, and M. Sendtner. 2002. Missense mutation in the *tubulin-specific chaperone E* (*Tbce*) gene in the mouse mutant *progressive motor neuronopathy*, a model of human motoneuron disease. *J. Cell Biol.* 159:563–569. http://dx.doi.org/10.1083/jcb.200208001

Cafferty, W.B., A.W. McGee, and S.M. Strittmatter. 2008. Axonal growth therapeutics: regeneration or sprouting or plasticity? *Trends Neurosci.* 31:215–220. http://dx.doi.org/10.1016/j.tins.2008.02.004

Charbaut, E., P.A. Curmi, S. Ozon, S. Lachkar, V. Redeker, and A. Sobel. 2001. Stathmin family proteins display specific molecular and tubulin binding

properties. *J. Biol. Chem.* 276:16146–16154. http://dx.doi.org/10.1074/jbc.M010637200

Chauvin, S., F.E. Poulain, S. Ozon, and A. Sobel. 2008. Palmitoylation of stathmin family proteins domain A controls Golgi versus mitochondrial subcellular targeting. *Biol. Cell*. 100:577–589. http://dx.doi.org/10.1042/BC20070119

Collard, J.F., F. Côté, and J.P. Julien. 1995. Defective axonal transport in a transgenic mouse model of amyotrophic lateral sclerosis. *Nature*. 375:61–64. http://dx.doi.org/10.1038/375061a0

Daniels, M.P. 1973. Fine structural changes in neurons and nerve fibers associated with colchicine inhibition of nerve fiber formation in vitro. *J. Cell Biol.* 58:463–470. http://dx.doi.org/10.1083/jcb.58.2.463

Davis, S., and G.D. Yancopoulos. 1993. The molecular biology of the CNTF receptor. *Curr. Opin. Neurobiol.* 3:20–24. http://dx.doi.org/10.1016/0959-4388(93)90030-3

Giger, R.J., E.R. Hollis II, and M.H. Tuszynski. 2010. Guidance molecules in axon regeneration. *Cold Spring Harb. Perspect. Biol.* 2:a001867. http://dx.doi.org/10.1101/cshperspect.a001867

Götz, R., S. Wiese, S. Takayama, G.C. Camarero, W. Rossoll, U. Schweizer, J. Troppmair, S. Jablonka, B. Holtmann, J.C. Reed, et al. 2005. Bag1 is essential for differentiation and survival of hematopoietic and neuronal cells. *Nat. Neurosci.* 8:1169–1178. http://dx.doi.org/10.1038/nn1524

Hafezparast, M., R. Klocke, C. Ruhrberg, A. Marquardt, A. Ahmad-Annuar, S. Bowen, G. Lalli, A.S. Witherden, H. Hummerich, S. Nicholson, et al. 2003. Mutations in dynein link motor neuron degeneration to defects in retrograde transport. *Science*. 300:808–812. http://dx.doi.org/10.1126/science.1083129

Hellal, F., A. Hurtado, J. Ruschel, K.C. Flynn, C.J. Laskowski, M. Umlauf, L.C. Kapitein, D. Strikis, V. Lemmon, J. Bixby, et al. 2011. Microtubule stabilization reduces scarring and causes axon regeneration after spinal cord injury. *Science*. 331:928–931. http://dx.doi.org/10.1126/science.1201148

Henderson, C.E., H.S. Phillips, R.A. Pollock, A.M. Davies, C. Lemeulle, M. Armanini, L. Simmons, B. Moffet, R.A. Vandlen, and L. Simmons. 1994. GDNF: a potent survival factor for motoneurons present in peripheral nerve and muscle. *Science*. 266:1062–1064. http://dx.doi.org/10.1126/science.7973664

Higuero, A.M., L. Sánchez-Ruiloba, L.E. Doglio, F. Portillo, J. Abad-Rodríguez, C.G. Dotti, and T. Iglesias. 2010. Kidins220/ARMS modulates the activity of microtubule-regulating proteins and controls neuronal polarity and development. *J. Biol. Chem.* 285:1343–1357. http://dx.doi.org/10.1074/jbc.M109.024703

Horvath, C.M., Z. Wen, and J.E. Darnell Jr. 1995. A STAT protein domain that determines DNA sequence recognition suggests a novel DNA-binding domain. *Genes Dev.* 9:984–994. http://dx.doi.org/10.1101/gad.9.8.984

Jeanneteau, F., K. Deinhardt, G. Miyoshi, A.M. Bennett, and M.V. Chao. 2010. The MAP kinase phosphatase MKP-1 regulates BDNF-induced axon branching. *Nat. Neurosci.* 13:1373–1379. http://dx.doi.org/10.1038/nn.2655

Kretzschmar, A.K., M.C. Dinger, C. Henze, K. Brocke-Heidrich, and F. Horn. 2004. Analysis of Stat3 (signal transducer and activator of transcription 3) dimerization by fluorescence resonance energy transfer in living cells. *Biochem. J.* 377:289–297. http://dx.doi.org/10.1042/BJ20030708

LaMonte, B.H., K.E. Wallace, B.A. Holloway, S.S. Shelly, J. Ascaño, M. Tokito, T. Van Winkle, D.S. Howland, and E.L. Holzbaur. 2002. Disruption of dynein/dynactin inhibits axonal transport in motor neurons causing late-onset progressive degeneration. *Neuron*. 34:715–727. http://dx.doi.org/10.1016/S0896-6273(02)00696-7

Lois, C., E.J. Hong, S. Pease, E.J. Brown, and D. Baltimore. 2002. Germline transmission and tissue-specific expression of transgenes delivered by lentiviral vectors. *Science*. 295:868–872. http://dx.doi.org/10.1126/science.1067081

Martin, N., J. Jaubert, P. Gounon, E. Salido, G. Haase, M. Szatanik, and J.L. Guénet. 2002. A missense mutation in Tbce causes progressive motor neuronopathy in mice. *Nat. Genet.* 32:443–447. http://dx.doi.org/10.1038/ng1016

Mitsumoto, H., K. Ikeda, T. Holmlund, T. Greene, J.M. Cedarbaum, V. Wong, and R.M. Lindsay. 1994. The effects of ciliary neurotrophic factor on motor dysfunction in wobbler mouse motor neuron disease. *Ann. Neurol.* 36:142–148. http://dx.doi.org/10.1002/ana.410360205

Ng, D.C., B.H. Lin, C.P. Lim, G. Huang, T. Zhang, V. Poli, and X. Cao. 2006. Stat3 regulates microtubules by antagonizing the depolymerization activity of stathmin. *J. Cell Biol.* 172:245–257. http://dx.doi.org/10.1083/jcb.200503021

Ng, D.C., I.H. Ng, Y.Y. Yeap, B. Badrian, T. Tsoutsman, J.R. McMullen, C. Semsarian, and M.A. Bogoyevitch. 2011. Opposing actions of extracellular signal-regulated kinase (ERK) and signal transducer and activator of transcription 3 (STAT3) in regulating microtubule stabilization during cardiac hypertrophy. *J. Biol. Chem.* 286:1576–1587. http://dx.doi.org/10.1074/jbc.M110.128157

Nishimune, H., S. Vasseur, S. Wiese, M.C. Birling, B. Holtmann, M. Sendtner, J.L. Iovanna, and C.E. Henderson. 2000. Reg-2 is a motoneuron neurotrophic factor and a signalling intermediate in the CNTF survival pathway. *Nat. Cell Biol.* 2:906–914. http://dx.doi.org/10.1038/35046558

Parvari, R., E. Hershkovitz, N. Grossman, R. Gorodischer, B. Loeys, A. Zecic, G. Mortier, S. Gregory, R. Sharony, M. Kambouris, et al; HRD/Autosomal Recessive Kenny-Caffey Syndrome Consortium. 2002. Mutation of TBCE causes hypoparathyroidism-retardation-dysmorphism and autosomal recessive Kenny-Caffey syndrome. *Nat. Genet.* 32:448–452. http://dx.doi.org/10.1038/ng1012

Poulain, F.E., S. Chauvin, R. Wehrlé, M. Desclaux, J. Mallet, G. Vodjdani, I. Dusart, and A. Sobel. 2008. SCLIP is crucial for the formation and development of the Purkinje cell dendritic arbor. *J. Neurosci.* 28:7387–7398. http://dx.doi.org/10.1523/JNEUROSCI.1942-08.2008

Puls, I., C. Jonnakuty, B.H. LaMonte, E.L. Holzbaur, M. Tokito, E. Mann, M.K. Floeter, K. Bidus, D. Drayna, S.J. Oh, et al. 2003. Mutant dynactin in motor neuron disease. *Nat. Genet.* 33:455–456. http://dx.doi.org/10.1038/ng1123

Pun, S., A.F. Santos, S. Saxena, L. Xu, and P. Caroni. 2006. Selective vulnerability and pruning of phasic motoneuron axons in motoneuron disease alleviated by CNTF. *Nat. Neurosci.* 9:408–419. http://dx.doi.org/10.1038/nn1653

Rajan, P., and R.D. McKay. 1998. Multiple routes to astrocytic differentiation in the CNS. *J. Neurosci.* 18:3620–3629.

Reid, E., M. Kloos, A. Ashley-Koch, L. Hughes, S. Bevan, I.K. Svenson, F.L. Graham, P.C. Gaskell, A. Dearlove, M.A. Pericak-Vance, et al. 2002. A kinesin heavy chain (KIF5A) mutation in hereditary spastic paraplegia (SPG10). *Am. J. Hum. Genet.* 71:1189–1194. http://dx.doi.org/10.1086/344210

Rogers, M.L., I. Atmosukarto, D.A. Berhanu, D. Matusica, P. Macardle, and R.A. Rush. 2006. Functional monoclonal antibodies to p75 neurotrophin receptor raised in knockout mice. *J. Neurosci. Methods*. 158:109–120. http://dx.doi.org/10.1016/j.jneumeth.2006.05.022

Sagot, Y., M. Dubois-Dauphin, S.A. Tan, F. de Bilbao, P. Aebischer, J.C. Martinou, and A.C. Kato. 1995. Bcl-2 overexpression prevents motoneuron cell body loss but not axonal degeneration in a mouse model of a neurodegenerative disease. *J. Neurosci.* 15:7727–7733.

Sagot, Y., S.A. Tan, J.P. Hammang, P. Aebischer, and A.C. Kato. 1996. GDNF slows loss of motoneurons but not axonal degeneration or premature death of pmn/pmn mice. *J. Neurosci.* 16:2335–2341.

Sagot, Y., T. Rossé, R. Vejsada, D. Perrelet, and A.C. Kato. 1998. Differential effects of neurotrophic factors on motoneuron retrograde labeling in a murine model of motoneuron disease. *J. Neurosci.* 18:1132–1141.

Schaefer, M.K., H. Schmalbruch, E. Buhler, C. Lopez, N. Martin, J.L. Guénet, and G. Haase. 2007. Progressive motor neuronopathy: a critical role of the tubulin chaperone TBCE in axonal tubulin routing from the Golgi apparatus. *J. Neurosci.* 27:8779–8789. http://dx.doi.org/10.1523/JNEUROSCI.1599-07.2007

Schmitt-John, T., C. Drepper, A. Mussmann, P. Hahn, M. Kuhlmann, C. Thiel, M. Hafner, A. Lengeling, P. Heimann, J.M. Jones, et al. 2005. Mutation of Vps54 causes motor neuron disease and defective spermiogenesis in the wobbler mouse. *Nat. Genet.* 37:1213–1215. http://dx.doi.org/10.1038/ng1661

Schweizer, U., J. Gunnersen, C. Karch, S. Wiese, B. Holtmann, K. Takeda, S. Akira, and M. Sendtner. 2002. Conditional gene ablation of Stat3 reveals differential signaling requirements for survival of motoneurons during development and after nerve injury in the adult. *J. Cell Biol.* 156:287–297. http://dx.doi.org/10.1083/jcb.200107009

Sellin, M.E., P. Holmfeldt, S. Stenmark, and M. Gullberg. 2008. Op18/Stathmin counteracts the activity of overexpressed tubulin-disrupting proteins in a human leukemia cell line. *Exp. Cell Res.* 314:1367–1377. http://dx.doi.org/10.1016/j.yexcr.2007.12.018

Sendtner, M., G.W. Kreutzberg, and H. Thoenen. 1990. Ciliary neurotrophic factor prevents the degeneration of motor neurons after axotomy. *Nature*. 345:440–441. http://dx.doi.org/10.1038/345440a0

Sendtner, M., H. Schmalbruch, K.A. Stöckli, P. Carroll, G.W. Kreutzberg, and H. Thoenen. 1992. Ciliary neurotrophic factor prevents degeneration of motor neurons in mouse mutant progressive motor neuronopathy. *Nature*. 358:502–504. http://dx.doi.org/10.1038/358502a0

Sendtner, M., B. Holtmann, and R.A. Hughes. 1996. The response of motoneurons to neurotrophins. *Neurochem. Res.* 21:831–841. http://dx.doi.org/10.1007/BF02532307

Sendtner, M., R. Götz, B. Holtmann, and H. Thoenen. 1997. Endogenous ciliary neurotrophic factor is a lesion factor for axotomized motoneurons in adult mice. *J. Neurosci.* 17:6999–7006.

Simon, C.M., S. Jablonka, R. Ruiz, L. Tabares, and M. Sendtner. 2010. Ciliary neurotrophic factor-induced sprouting preserves motor function in a mouse model of mild spinal muscular atrophy. *Hum. Mol. Genet.* 19:973–986. http://dx.doi.org/10.1093/hmg/ddp562

Suh, L.H., S.F. Oster, S.S. Soehrman, G. Grenningloh, and D.W. Sretavan. 2004. L1/Laminin modulation of growth cone response to EphB triggers growth pauses and regulates the microtubule destabilizing protein SCG10. *J. Neurosci.* 24:1976–1986. http://dx.doi.org/10.1523/JNEUROSCI.1670-03.2004

Tararuk, T., N. Ostman, W. Li, B. Björkblom, A. Padzik, J. Zdrojewska, V. Hongisto, T. Herdegen, W. Konopka, M.J. Courtney, and E.T. Coffey. 2006. JNK1 phosphorylation of SCG10 determines microtubule dynamics and axodendritic length. *J. Cell Biol.* 173:265–277. http://dx.doi.org/10.1083/jcb.200511055

Verma, N.K., J. Dourlat, A.M. Davies, A. Long, W.Q. Liu, C. Garbay, D. Kelleher, and Y. Volkov. 2009. STAT3-stathmin interactions control microtubule dynamics in migrating T-cells. *J. Biol. Chem.* 284:12349–12362. http://dx.doi.org/10.1074/jbc.M807761200

Watabe-Uchida, M., K.A. John, J.A. Janas, S.E. Newey, and L. Van Aelst. 2006. The Rac activator DOCK7 regulates neuronal polarity through local phosphorylation of stathmin/Op18. *Neuron*. 51:727–739. http://dx.doi.org/10.1016/j.neuron.2006.07.020

Wiese, S., T. Herrmann, C. Drepper, S. Jablonka, N. Funk, A. Klausmeyer, M.L. Rogers, R. Rush, and M. Sendtner. 2010. Isolation and enrichment of embryonic mouse motoneurons from the lumbar spinal cord of individual mouse embryos. *Nat. Protoc.* 5:31–38. http://dx.doi.org/10.1038/nprot.2009.193

Witte, H., D. Neukirchen, and F. Bradke. 2008. Microtubule stabilization specifies initial neuronal polarization. *J. Cell Biol.* 180:619–632. http://dx.doi.org/10.1083/jcb.200707042

Yu, W., C. Ling, and P.W. Baas. 2001. Microtubule reconfiguration during axogenesis. *J. Neurocytol.* 30:861–875. http://dx.doi.org/10.1023/A:1020622530831

Zhao, C., J. Takita, Y. Tanaka, M. Setou, T. Nakagawa, S. Takeda, H.W. Yang, S. Terada, T. Nakata, Y. Takei, et al. 2001. Charcot-Marie-Tooth disease type 2A caused by mutation in a microtubule motor KIF1Bbeta. *Cell*. 105:587–597. http://dx.doi.org/10.1016/S0092-8674(01)00363-4